GATE AREA RAINFALL ESTIMATION FROM SATELLITE IMAGES

A REPORT

from the space science and engineering center
the university of wisconsin-madison
madison, wisconsin

GATE AREA RAINFALL ESTIMATION FROM SATELLITE IMAGES

David W. Martin
John Stout

Space Science and Engineering Center
The University of Wisconsin-Madison

Dhirendra N. Sikdar

Geological Sciences Department
The University of Wisconsin-Milwaukee

July 1975

A Report on NOAA Grant 04-5-158-47

TABLE OF CONTENTS

ACKNOWLEDGEMENTS

Tony Schreiner assisted in data analysis. Figures were capably drafted by Dana Wooldridge. Mrs. Barbara Mueller typed the text. Gary Chatters provided technical assistance.

1. OVERVIEW

This interim report reviews progress on a rainfall estimation program begun in 1973 in collaboration with NOAA's Experimental Meteorology Laboratory.* The aim of the program is to develop and apply a method for estimating GATE-area rainfall from geosynchronous satellite images. Its basis is a pair of observations familiar to cloud watchers, that in general thick cumulus clouds reflect more light than thin cumulus clouds; they also tend to be wetter. Hence, for cumulus clouds of a given size viewed from a satellite, the higher the brightness, the heavier the rain.

Going one step further, many observers have noted a time dependence in the relationship between rainfall and cloud brightness. Two clouds of the same area can have quite different rain rates if one is young and the other old. For cumulonimbi--the most important tropical rainmakers--rainfall is heaviest in the earlier stages of evolution, before cloud area peaks. Our method therefore incorporates stage of development in addition to cloud brightness and area as estimators of rainfall. These relations are illustrated in Figure 1.

Activity in the program is shifting from development toward the second program objective--estimation of rainfall in the GATE area. Before such estimates can be made it is necessary to recalibrate the method from the ATS visible images used in its development to the SMS visible and infrared images which cover the GATE area. The cloud area-rainfall relationships developed for Florida must also be tested and modified as necessary for the GATE area. For this we plan to use as ground truth calibrated radar data

---

*The Experimental Meteorology Laboratory has been merged with the National Hurricane Center to form the National Hurricane and Experimental Meteorology Laboratory. Our collaboration is with the Cumulus Group, NHEML.

from two GATE ships, the Researcher and the Oceanographer. In the sections which follow we review the status of the method. This review is followed by results of ATS-SMS equivalence measurements. We present results of comparisons between radar images and SMS visible and infrared images over Florida, then describe tests designed to assess accuracies of the method in the estimation of GATE area rainfall.

II. METHOD

Earlier contract reports (Martin and Sikdar, 1973, 1974) describe the development of this method. A recent comprehensive account is given in an NHEML Technical Note, "Rainfall Estimation from Geosynchronous Satellite Imagery During Daylight Hours," by Woodley and Griffith (manuscript, 1975); this Note also describes many tests of the method.

When this work began in 1972 data were available from the third Applications Technology Satellite (ATS-3) and from two 10-cm radars in south Florida. These data became the base for establishing cloud brightness thresholds distinguishing wet and dry clouds, also for deriving time dependent relations between cloud area and echo area, and between cloud area and volumetric rainfall rate.

Taking advantage of EML's summer convection experiments, special radar and satellite data sets were gathered for the summers of 1972, 1973, and 1974. These include digital radar tapes from the National Hurricane Center WSR-57 radar (1973 and 1974), and digital satellite tapes from ATS-3 (three summers) and from SMS-1 (1974). For selected days radar images were matched in time to satellite images, then displayed as a registered sequence on a video display and processing device. The corresponding satellite images were navigated, remapped to the scale and projection of the radar images, and

displayed as a sequence on adjacent frames. Clouds and corresponding echoes were outlined for computer measurement of areas. Sample plots of cloud area, echo area, and volumetric rainfall for an ATS-3 cloud are given in Figure 2. Combining such measurements for many clouds, and normalizing cloud and echo area, gives the curve--called a cloud-echo area diagram--needed for estimating rain from a series of measurements of cloud area. With the provision of digital radar data we began to calculate volumetric rainfall as well as echo area. A second type of curve--referred to as a cloud area-rainfall diagram--relates cloud area to volumetric rainfall rate, so eliminating the intermediate step involving echo area.

In developing such diagrams we prefer to work with digital magnetic tape rather than photographic hard copy data: the digital tape format gives us better resolution, tighter control on signal levels, and greater flexibility in formatting data for display. The advantages this offers in measurement accuracy and precision are very important, for they substantially reduce the level of noise in our measurements, and therefore the number of measurements needed before the signal can be well and truly separated from the noise.

Measurements are made on the Man-Computer Interactive Data Access System (McIDAS). This is an image storage, display, and processing system consisting of four sections--data archive, data access, video display, and operator console--each linked to and controlled by a central, dedicated computer. Details of system configuration and operation are given by Smith (1975) and Chatters and Suomi (1975). Capabilities used in this program are the following:

(1) Variable rate, variable length movie loop display of image sequences.

This facilitates identification and tracking of discrete cloud-echo systems.

(2) Instant, infinitely variable black and white and color enhancement. Enhancement further aids identification and tracking of discrete cloud-echo systems.

(3) Rapid frame load. Images found to be out of registration can be reloaded at the proper locations--one minute or less per frame.

(4) Independent signal tracks, instant transfer, and dual image display. A radar sequence and corresponding satellite sequence can be loaded opposite one another on separate video tracks and individually enhanced. Transfer from one to another is instantaneous--a single key-in is all that is needed; simultaneous display (through an interlacing of alternate picture elements) is accomplished by hitting another key. The association of particular clouds with corresponding echoes is made easier and more accurate.

(5) Brightness normalization. Visible images can be brightness normalized to a standard (operator specified) sun-satellite geometry. Effects of changing sun angles are made negligible over a period (up to 8 hours) comparable to the lifetimes of small mesoscale convective systems. This normalization scheme is described in Appendix B.

(6) Draw mode. Outlines can be drawn to the irregular shapes of clouds and echoes, for precise measurement of areas.

(7) Area statistics. Results of an area measurement (maximum brightness, latitude and longitude, and area above up to eight operator specified brightness thresholds) appear in seconds on a CRT at the operator's console. Results can be checked as measurements are made. Area

statistics and cloud outlines are stored on file. They can be printed, written on tape, or displayed for editing as overlays on the original image. Overlapping outlines, omissions, and other mistakes can be found and corrected immediately.

III. ATS-SMS EQUIVALENCE

In order to combine area statistics from ATS and SMS data, we need to relate the respective digital levels used as thresholds to define clouds. Since ATS-3 data are brightness normalized to a Florida reference point in space and time (Miami-25°43'N,80°15'W,2 Jul 1973,1716 Z) and SMS-1 to a GATE reference point (center of B-array-08°30'N,23°30'W, 4 Aug 1974, 1330 Z) we only need relate levels once.

This problem could be approached from an instrument design and signal chain point of view. We chose instead to work with the data itself and employ a measure used in our rain estimation--cloud area above a threshold brightness. The advantage of working with the digital data is that one is downstream of any undocumented influences on the signal. An area approach is superior to one involving single pixels because the effects of differences in sensor resolution and of differences in response among the eight SMS visible channels (Bauer and Lienesch, 1975) are averaged out.

To equivalence digital levels through area measurement we find a large cloud or cloud cluster viewed by both satellites within a few minutes of each other. Images from each satellite are normalized to their respective reference points. Then with closed brightness contours, equivalent levels will enclose equal areas.

Results for the three days analyzed are seen in Figure 3. Each curve represents the correspondence of ATS-SMS digital brightness for equal areas

of a single cloud. Curves for the same day tend to cluster. The strong concavity of curves for four clouds on day 181 is a result of slow sensor response on ATS to decreasing scene brightness, when the satellites scanned unusually bright clouds contrasting sharply with a dark cloud free background. Excepting these concave curves, the curves for day 248 tend to be higher than those for other days. There are two reasons for this: ATS signal levels, as measured by alpha values (see Appendix A), had dropped some 20 percent; and, second, for the clouds selected the effect "striping" - uneven response of the seven operating visible channels on SMS - was particularly strong (Bauer and Lienesch, 1975; see also Figure 4).

Also shown in Figure 3 is a theoretical curve obtained by equivalencing ATS-3 brightness levels to SMS-1 brightness levels through the normalization tables of brightness versus optical thickness for each reference point (see Appendix B). This curve is similar in shape and position to the area equivalence curves.

It is the first set of curves, for day 181, that contributed most strongly to the selection of 172 digital counts as the level which best matches the ATS digital level of 60 previously used for defining clouds. Later results, from day 191 especially, indicate a lower level might be better. We will return to this point in the discussion of cloud area and rainfall comparisons.

This procedure establishes a correspondence between normalized ATS-3 and SMS-1 data for a portion of the summer period, 1974. To legitimately extend this to 1973 ATS-3 data, it must be established that the ATS-3 signal was constant from 1973 through this period in 1974. Evidence that this is true (except for day 248, as noted previously) is presented in Appendix A. It is also implied in this approach that SMS visible channel signal levels held steady over the comparison period. Calibrations made for four widely

spaced days in the summer of 1974 show a 25 percent variability. This is consistent with indications based on ground station monitoring that signal levels on the visible channels of SMS remained essentially constant over the period of GATE (Goddard and Remondi, 1975; Bauer and Lienesch, 1975).

IV. SMS-RADAR COMPARISONS

A key step in extending rain estimates to nighttime hours is adapting the method to infrared data. To do this we have repeated for two days the satellite-radar sequence comparisons over Florida, this time using SMS rather than ATS images (Figure 5). Although the primary purpose of such comparisons is to establish cloud area-echo area-rain volume relations for infrared data, SMS visible cloud areas also are compared with echo areas. These comparisons enlarge the data base for specifying the cloud area-echo area-rain volume relation, serve as a verification case for the ATS-SMS brightness equivalence relation, and provide a background for analyzing the infrared sequences.

Results for the visible cloud-echo comparisons are surveyed in Figure 6a and b, showing two clouds from the 14 that were tracked on day 216 (4 August), and Figure 7a and b, showing two clouds from the 9 that were tracked on day 248 (5 September). We note from these two dozen cloud plots that cloud area tends to peak earlier, by up to one hour, at higher brightness levels. Likewise, echo area peaks earlier at higher brightness (reflectivity) levels, and in general leads cloud area by up to one hour. Integrating these phase effects of echo area in rain volume produces a distinct phase difference--typically one half to one and one half hours--between maxima in volumetric rainfall and cloud area . Volumetric rainfall plots tend to be skewed toward the right, indicating that growth occurs over a shorter period than dissipation. Cloud area plots show little tendency to skew; their shape is like a Gaussian curve. These features were also characteristic

of cloud-echo area plots for ATS-3.

Analyzing the infrared cloud-echo sequences proved to be more difficult. Brightness was insufficient as a criterion for selection of precipitating convective clouds. Through comparisons with visible pictures, cloud growth was found to be an effective secondary criterion for eliminating passive cirrus. Because of the much inferior resolution of the infrared sensor (a factor of 8 less than visible resolution), and the strong obfuscating effect of cirrus at infrared wavelengths, only large or isolated convective systems could be followed through most of their lifetimes. In a few instances of cloud merger it was apparent from visible and infrared images that shearing cirrus formed a bridge between systems which convectively were well separated (see Figure 5). One result of these effects is a reduction in the number of trackable clouds from visible to corresponding infrared sequences. Coverage also tended to be less complete, because the larger and longer lived infrared clouds more often extended outside the radar area; the compensation for this was longer infrared sequences. Although available visible images were referred to for guidance, no attempt was made to isolate and follow exact infrared counterparts of the visible clouds that had already been tracked.

Plots of infrared cloud-echo area and volumetric rainfall, presented in Figures 8a and b and 9a and b show that there do exist consistent relations among infrared cloud area, echo area, and volumetric rainfall. These relations resemble those found for visible clouds. The principal differences from the visible are larger ratios of infrared cloud area to echo area (and rainfall) and a skewing of cloud area toward the right. Clouds in the infrared also are indentified at a later stage in the evolution of the convective system, usually

after rain had begun falling.

Infrared cloud areas referred to above are defined by the 160 digital count level. This was selected as an approximate match to the level, 172 digital counts, used to define clouds in the SMS visible [which in turn corresponds to the ATS-3 60 digital count level selected on the basis of precipitation probability (Martin and Sikdar, 1974)]. The 160 level also offers a compromise between the area truncation observed in "crowded" clouds at lower levels (Figure 9b), and the time truncation typical at higher levels. In our SMS data it typically lies within the region of strongest brightness gradient along the edge of anvils in tropical cumulonimbi.

The match of these two levels can best be seen in plots of area for individual clouds followed in both visible and infrared* (Figure 10). Visible cloud area has a flatter curve that tends to cover more of the rainfall profile.

Cloud plots for 4 August and 5 September are summarized as cloud area-rainfall diagrams in Figures 11 and 12. Patterns for visible clouds are similar on both days. Peaks in area normalized volumetric rainfall are left of center, confirming the phase lag of cloud area to rainfall noted earlier. Clouds are picked up at or slightly after the time rainfall begins; typically, rainfall ends long before the cloud has disappeared. For this threshold brightness (172 digital counts) three fourths or more of the total cloud rainfall occurs before cloud area peaks. One noteworthy difference between the two days is the higher ratio of rain volume to maximum cloud area on 4 August--clouds of a given area on this day were wetter.

---

*The number of such clouds is relatively small because of the aforementioned differences in sensor resolution and cloud sensitivity.

The infrared distributions are flatter and lower. The absence of a well defined peak indicates that the phase relation between maximum rainfall and maximum cloud area is more variable than for visible clouds. It is also clear that clouds are being picked up after the onset of precipitation. As in the case of the visible plots, 4 August shows a higher ratio of rain volume to maximum cloud area than 5 September.

An explanation for this difference between 4 August and 5 September lies in a stronger shear on 5 September. Vector differences of the 850 mb and 200 mb winds were of magnitude 23 m s^{-1} on 4 August and 35 m s^{-1} on 5 September. Marwitz (1972) and Foote and Fankhauser (1973) find that in cases of moderate to strong shear the precipitation efficiency of Great Plains thunderstorms is inversely related to vertical shear of the horizontal wind. In fact we find this dependence of rain volume to wind shear in comparisons between 1973 and 1974 cloud area-rainfall curves. The cloud area-volumetric rainfall curve based on 1973 data is higher than either of the 1974 curves. Vertical shear was correspondingly lower, averaging 16 m s^{-1} from 850 to 200 mb.*

These observations indicate that vertical shear can be a large modulating influence on rainfall in tropical cumulonimbi; hence an adjustment to rain estimates might be needed under conditions of weak or strong shear (as measured by soundings, cloud tracer winds, or the ellipticity of cirrus plumes). Curves for both years are combined (ignoring shear differences) in a single cloud area-rainfall diagram shown in Figure 13.

---

*The 1973-1974 area-rainfall difference was observed in spite of the bias towards smaller SMS cloud areas implicit in selection of 172 rather than some lower digital level as equivalent to 60 digital counts ATS. Thus the use of a relatively high 172 digital count level was more than compensated by stronger shear in 1974.

V. GATE PROCESSING

There has long been evidence of measurable differences between precipitation processes over land and sea. Early results from GATE indicate quite distinctive aerosol, cloud, and echo characteristics in the GATE area (Weickman, 1975; Simpson and Simpson, 1975; Scherer, personal communication, 1974). Although land-sea differences have not been apparent in the cases already analyzed over and adjacent to Florida, observations from GATE argue compellingly for limited testing before the method is used routinely to estimate GATE area rainfall.

The ground truth for such a test must come principally from the GATE 5-cm radars--no other measurement comes close to matching the time and space scale of the satellite. We plan to process digital data from one or two of the GATE radars just as we have for the NHEML radar, matching a several hours long radar sequence to the corresponding satellite sequence. Rainfall will be estimated independently for a range of well defined convective systems appearing in both the radar and satellite sequences. The results will determine adjustments or modifications to the method as it has been configured using Florida ground truth.

A prime candidate for this test is 5 September (day 248), one of the most active of all GATE days in the B-array. Five September is one of two priority days selected by CEDDA for early processing of Oceanographer and Researcher digital radar data. Present schedules call for delivery of processed tapes to the National Weather Records Center in June 1975, thus they should be available for analysis very early in fiscal year 1976. Five September has also been selected by SSEC for analysis as a wind set day, hence much of the SMS data for that day is already navigated and available

on save tapes. It is known to be of very high quality. Since the radar data are not needed for making the satellite estimate of rainfall, this part of the test is underway.

VI. SUMMARY

Several important steps have been taken this year.

- At NHEML the Cumulus Group has extensively tested a cloud area-echo area relation based on visible data from ATS-3. They found that the method provides daytime rainfall estimates accurate to a mean absolute factor of 1.5.
- At SSEC a tentative calibration has been established between Florida cloud brightness in ATS-3 and GATE area cloud brightness in SMS-1. With this calibration the ATS cloud area-echo area-rainfall relation can be modified for use with visible data from SMS-1.
- The first two infrared image sequences have been analyzed. In spite of differences in sensor resolution and response, these pictures contain the information needed to extend the cloud area-echo area-rainfall from visible images to infrared images, and thus to achieve full day and night coverage in rainfall estimation.
- These steps lead us to the last step prior to routine use of the method in estimating GATE rainfall: testing (and fine tuning) the GATE area SMS cloud area-echo area-rainfall relation against GATE ground truth. This test, and the processing to follow, are the subject of a follow-on proposal covering work in fiscal year 1976.

REFERENCES

Bauer, B. and J. Lienesch, 1975: VISSR Data Calibration. Central Processing and Analysis of Geostationary Satellite Data, NOAA Technical Memorandum NESS 64, 59-65.

Chatters, G. C. and V. E. Suomi, 1975: The Applications of McIDAS. IEEE Transactions on Geoscience Electronics, GE-13, 137-146.

Foote, G. B. and J. C. Fankhauser, 1973: Airflow and Moisture Budget Beneath a Northeast Colorado Hailstorm. J. Appl. Meteor., 12, 1330-1353.

Goddard, B. and B. Remondi, 1975: Diagnostic Tools for Quality Assessment of VISSR Data. Central Processing and Analysis of Geostationary Satellite Data, NOAA Technical Memorandum NESS 64, 48-58.

Martin, David W. and Dhirendra N. Sikdar, 1973: Calibration of ATS-3 Images for Quantitative Precipitation Estimation. Report on NOAA Contract 03-3-022-18, Space Science and Engineering Center, Univ. of Wisconsin, Madison.

_____, 1974: Rainfall Estimation from Satellite Images. Report on NOAA Contract 03-4-022-22, Space Science and Engineering Center, Univ. of Wisconsin, Madison.

Marwitz, J. D., 1972: Precipitation Efficiency of Thunderstorms on the High Plains. Preprints 3rd Conf. Wea. Modification, Rapid City, S. D., Amer. Meteor. Soc., 245-247.

Simpson, Joanne and Robert H. Simpson, 1975: Preliminary Scientific Results of the GARP Atlantic Tropical Experiment, GATE Report No. 14.

Smith, E. A., 1975: The McIDAS System. IEEE Transactions on Geoscience Electronics, GE-13, 123-136.

Weickman, Helmut, 1975: Preliminary Scientific Results of the GARP Atlantic Tropical Experiment, GATE Report No. 14.

Woodley, W. L. and C. G. Griffith, 1975: Rainfall Estimation from Geosynchronous Satellite Imagery During Daylight Hours. Preliminary Report, National Hurricane and Experimental Meteorology Laboratory, Coral Gables, FL, 116 p.

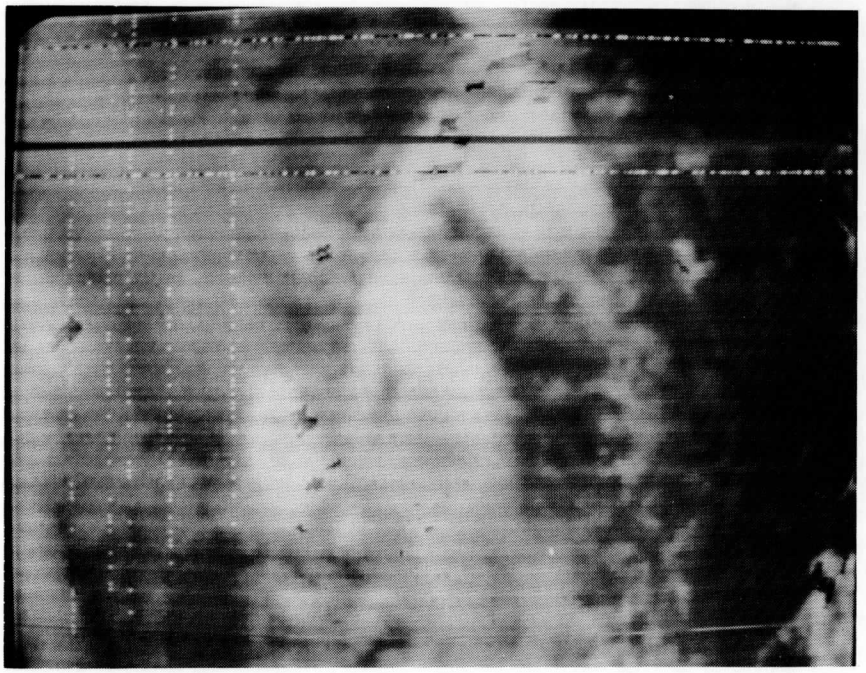

Figure 1 Full resolution visible image from SMS-1 centered on Miami, Florida; 1830 Z 5 September 1974. Echoes are found in the brighter cloud areas. Bright clouds without echoes show signs of decay; for example, the cloud in the center has a long southward pointing cirrus plume and is declining in area. (Rows and columns of white dots top and left side result from noise in the archived data; several missing lines appear as a dark horizontal band.)

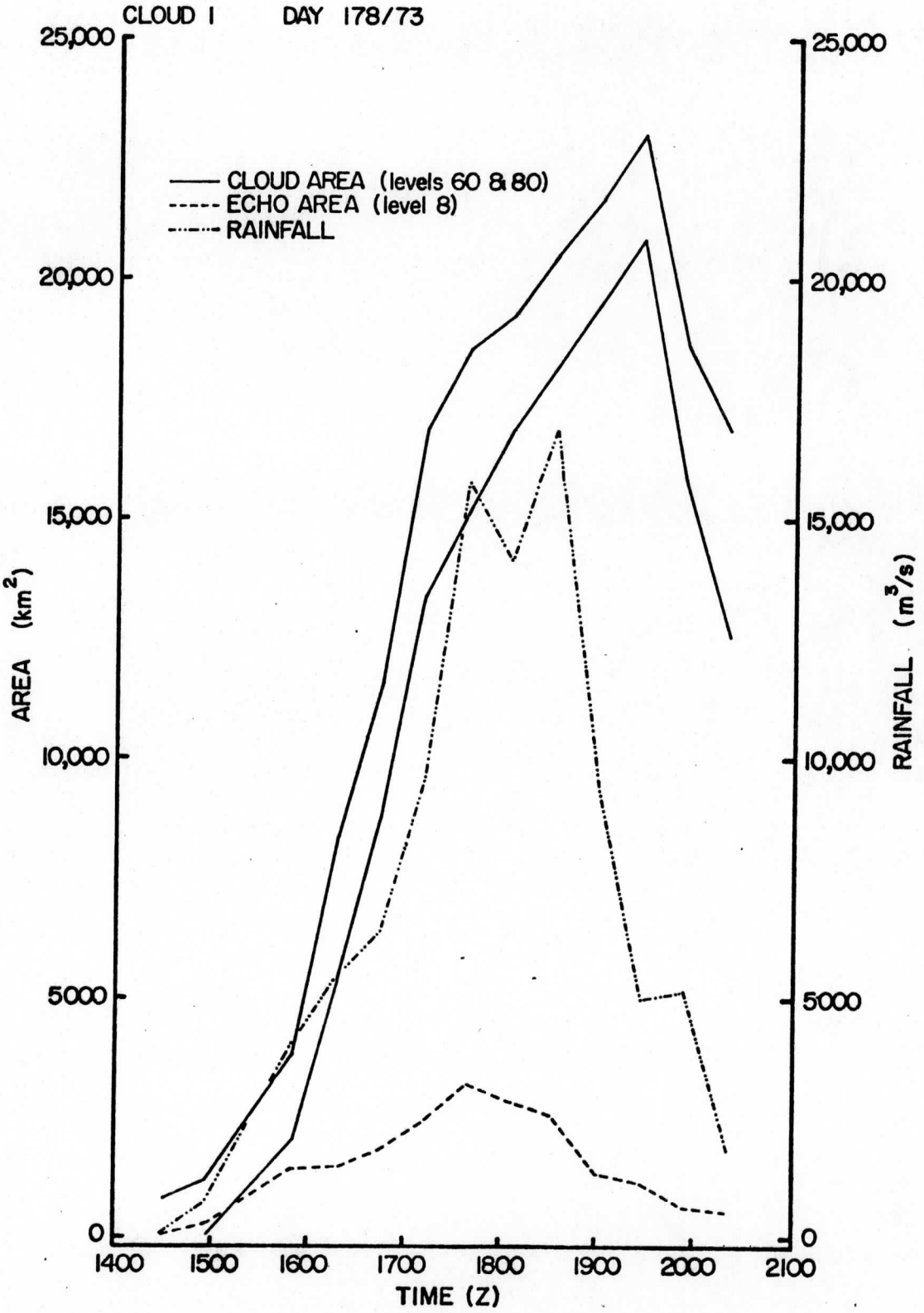

Figure 2 History of one south Florida cloud followed in ATS-3 images from 27 June 1973. Curves show area at two brightness levels, 60 and 80 digital counts, echo area, and volumetric rainfall.

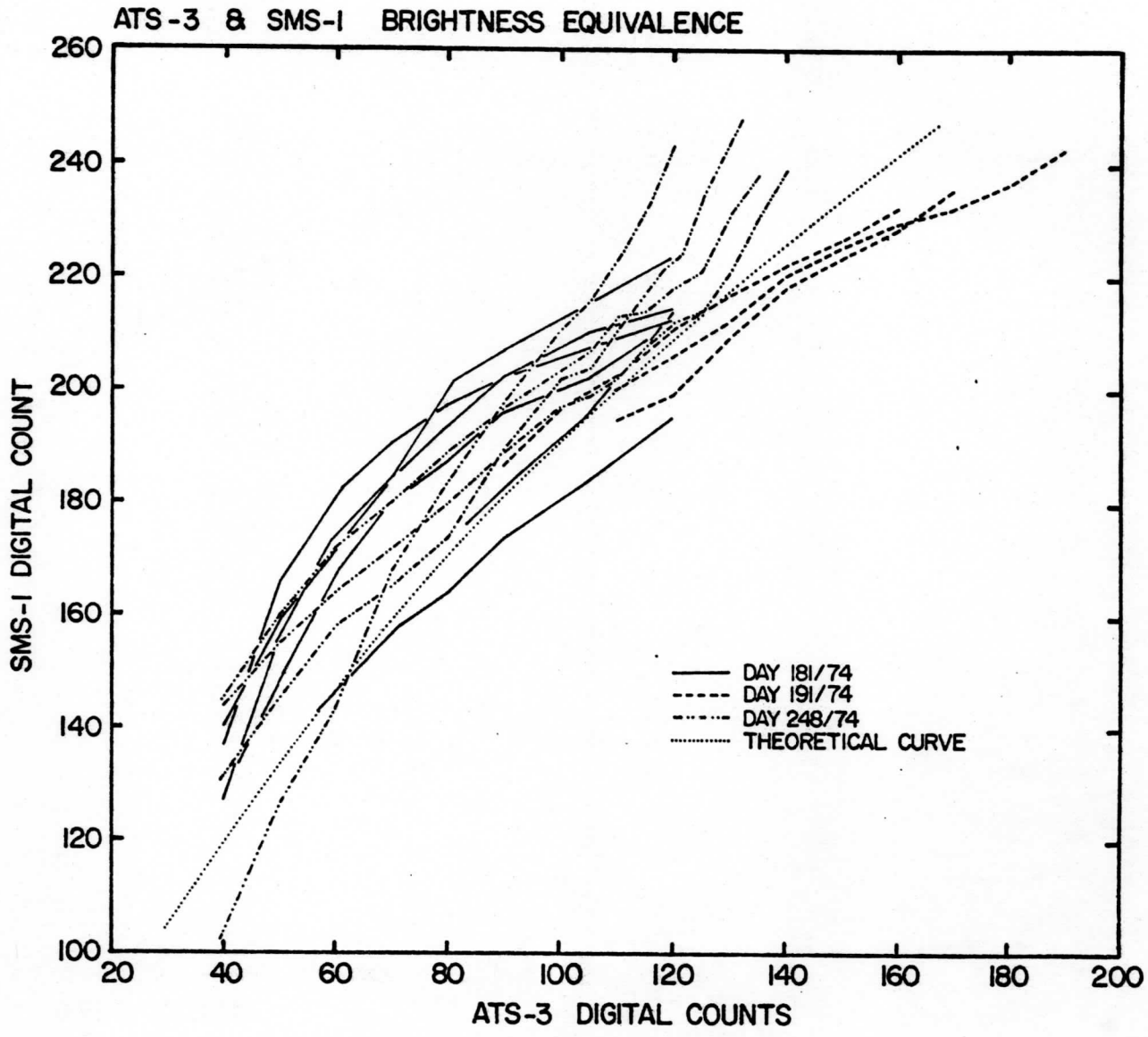

Figure 3 Equivalent brightness levels between ATS-3 and SMS-1 for individual clouds on three days in 1974; a theoretical curve is also shown. The theoretical curve was obtained by normalizing brightness levels from the ATS reference point to the SMS reference point.

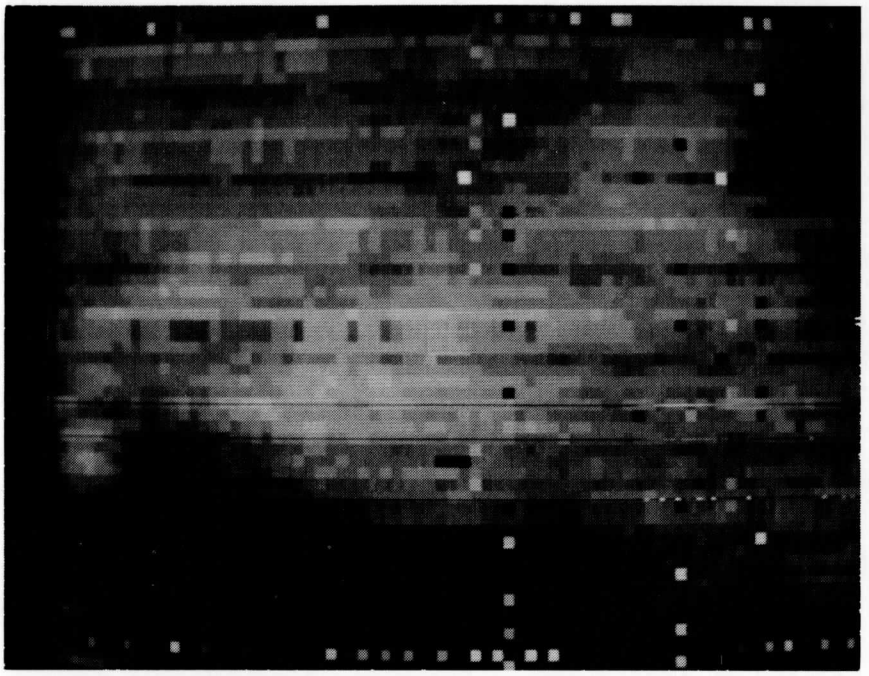

Figure 4 Blow-up of SMS-1 cloud used to equivalence levels on 5 September (day 181) 1974. Light and dark stripes of multiples of eight lines indicate a nonuniform response of the visible VISSR sensors to incident radiation.

1800 Z 216/74

Figure 5 Sample pictures from the 4 August (day 216) 1974 sequence. Miami is approximately centered in each frame. Visible clouds and outlines are shown at the top, infrared clouds and outlines at the bottom. Echoes appear as irregular dark spots in the lighter cloud area of the bottom frame. The visible picture is brightness normalized. Radar data were remapped to SMS projection and scale. Cloud systems are less well defined in the infrared, and cirrus forms bridges between some systems. For example, note infrared 107 and visible 9 and 18, to left of center.

Figure 6 Histories of two south Florida clouds followed in SMS-1 visible images from 4 August 1974. Cloud area, echo area, and volumetric rainfall are shown. Numbers next to cloud area curves represent digital counts. The curves for echo area correspond to rain rates of <1, 2, 12, and 38 mm/hr.
a. Cloud 1
b. Cloud 10

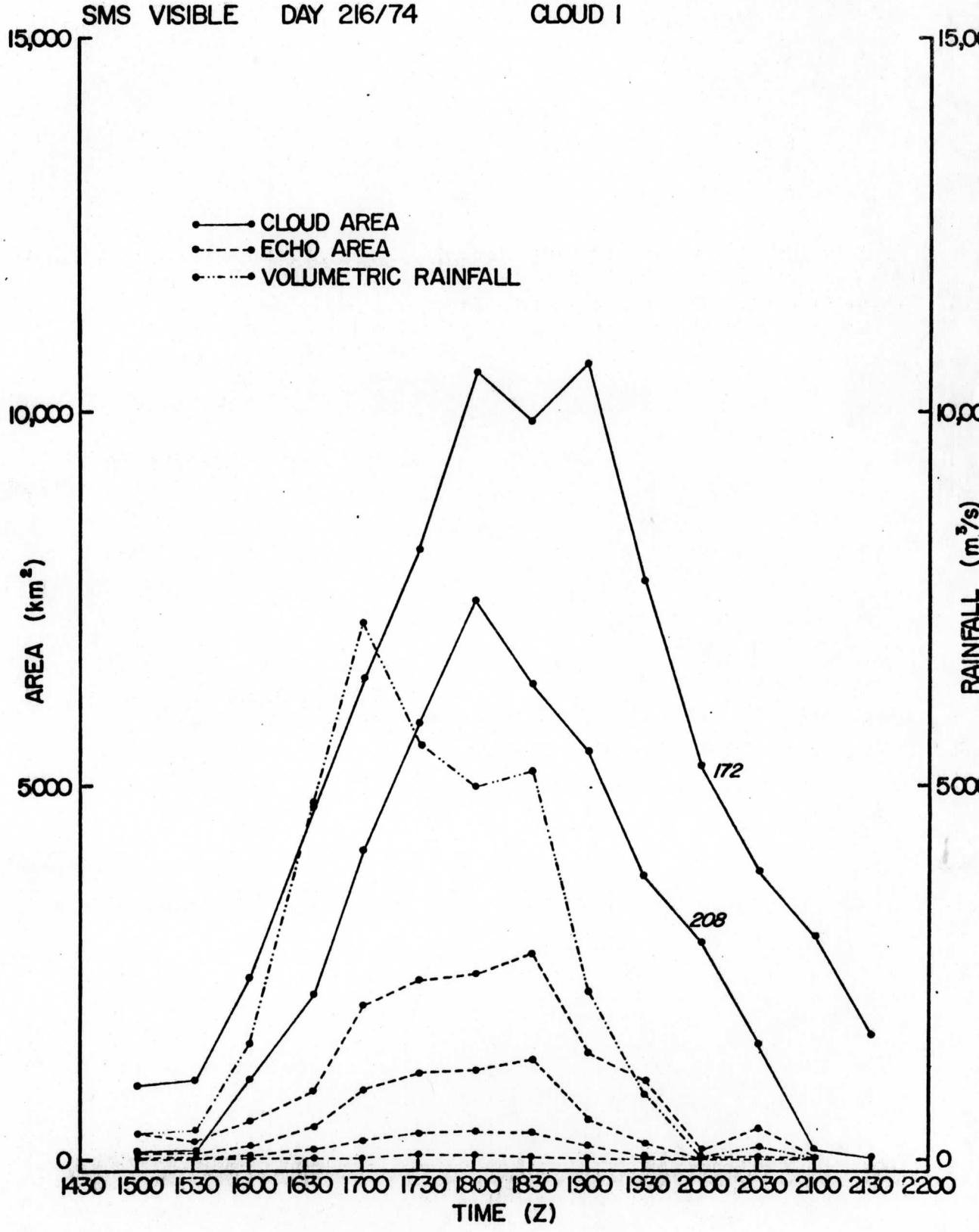

Figure 6a

Figure 6b

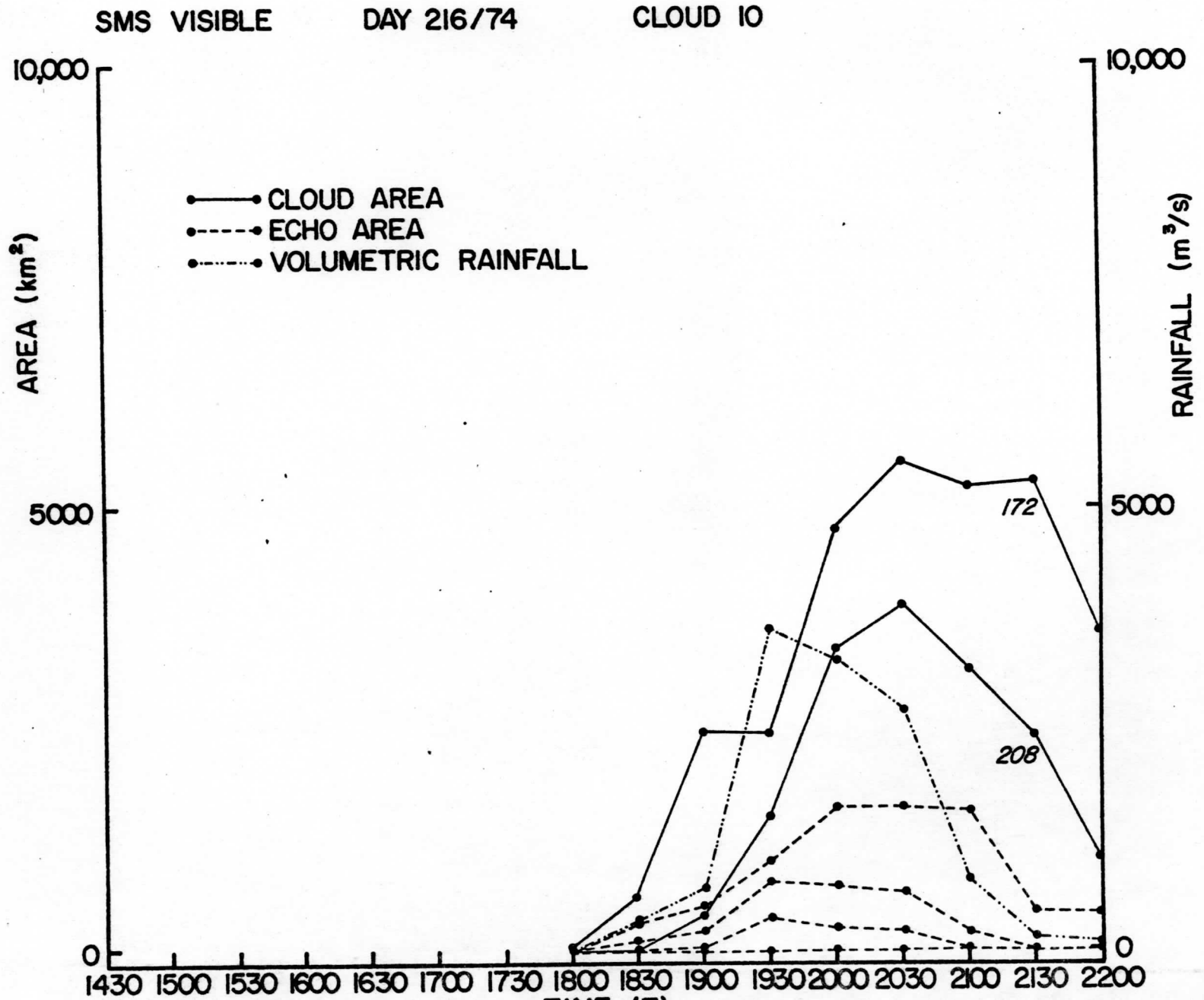
SMS VISIBLE
DAY 216/74
CLOUD 10
10,000
5000
0
AREA (km²)
RAINFALL (m³/s)
CLOUD AREA
ECHO AREA
VOLUMETRIC RAINFALL
172
208
1430 1500 1530 1600 1630 1700 1730 1800 1830 1900 1930 2000 2030 2100 2130 2200

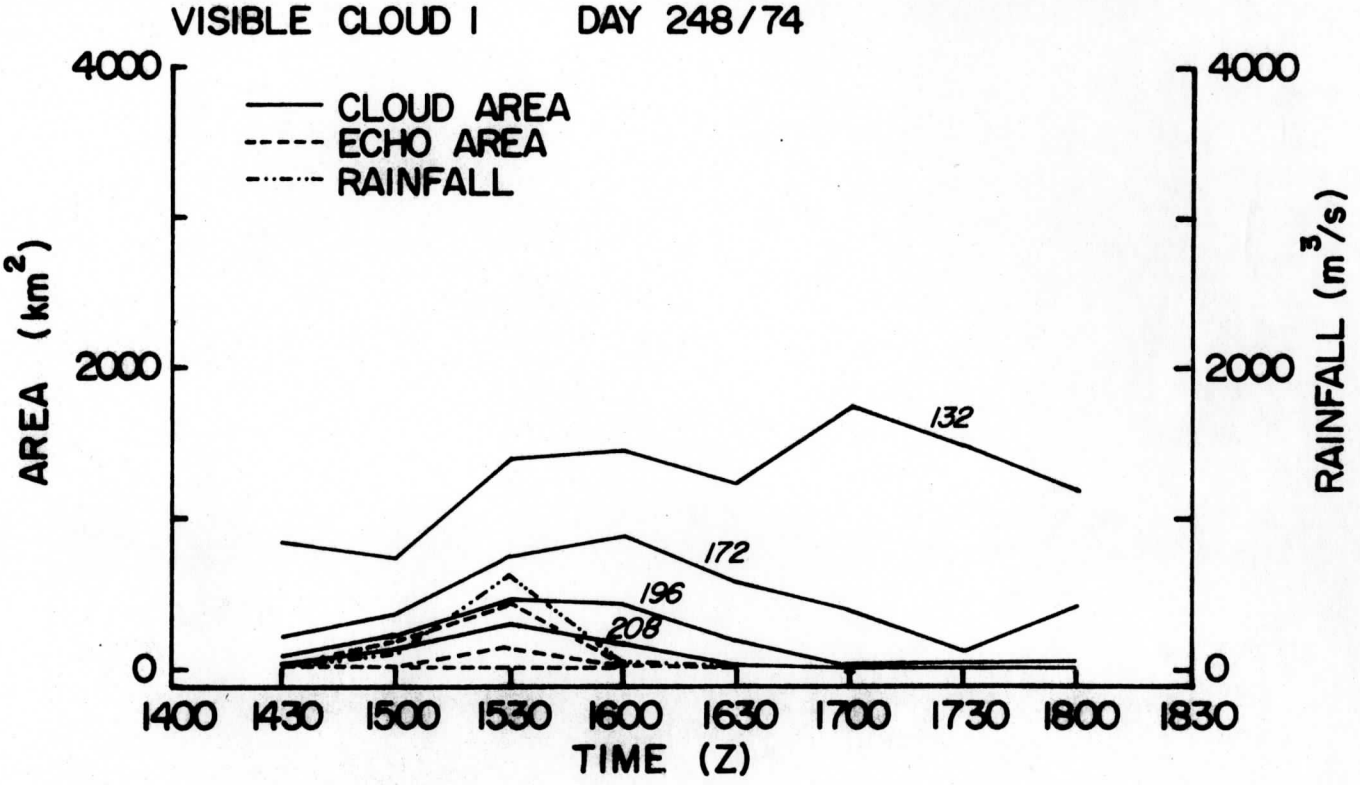

Figure 7a

Figure 7 Histories of two south Florida clouds followed in SMS-1 visible images from 5 September 1974. See Figure 6 for further information.
a. Cloud 1
b. Cloud 6

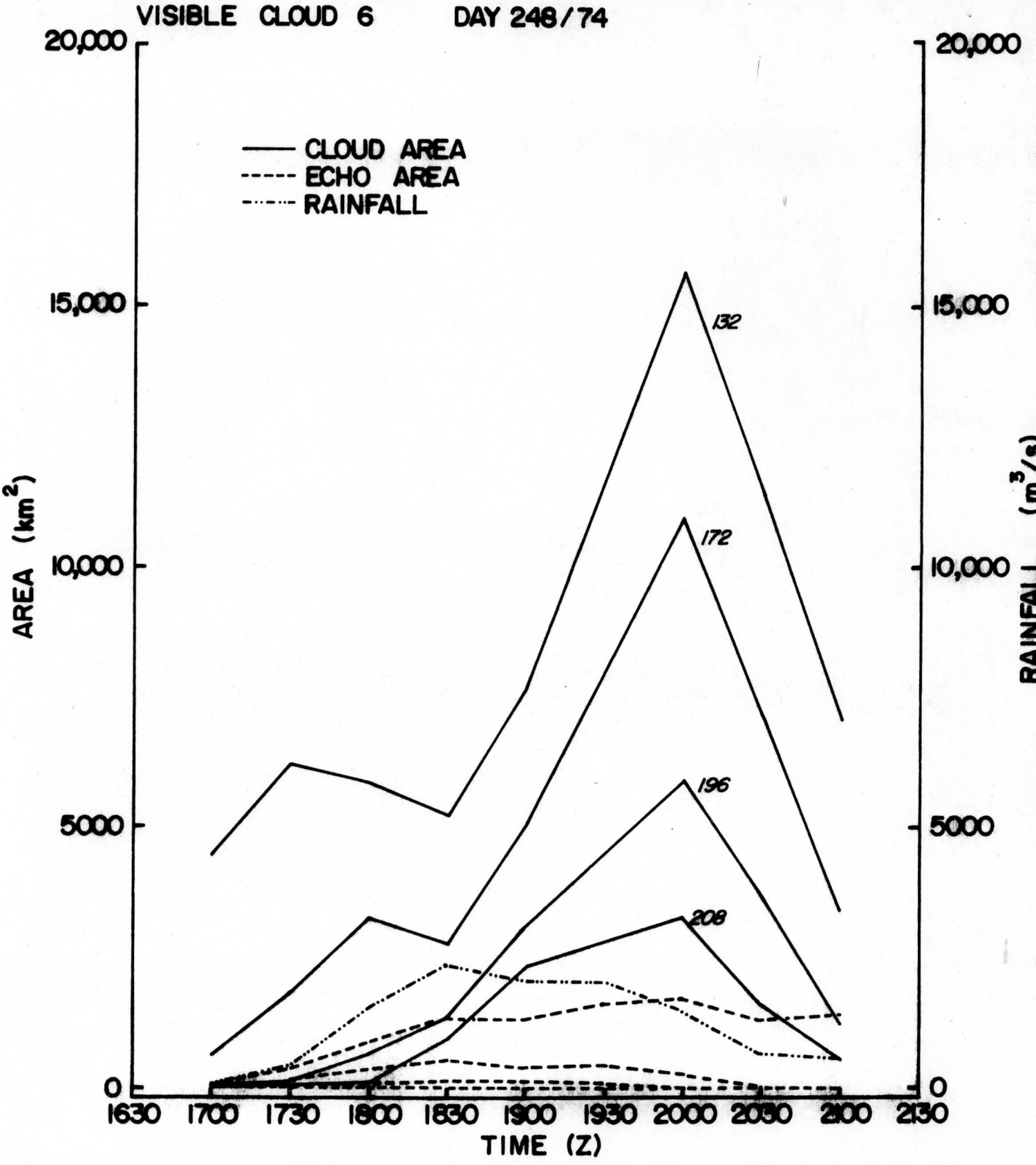
VISIBLE CLOUD 6 DAY 248/74
CLOUD AREA
ECHO AREA
RAINFALL
20,000
15,000
10,000
5000
0
AREA (km²)
132
172
196
208
1630 1700 1730 1800 1830 1900 1930 2000 2030 2100 2130
TIME (Z)

Figure 7b

Figure 8 Histories of two south Florida clouds followed in SMS-1 infrared images from 4 August 1974. See Figure 6 for further information.
a. Cloud 102
b. Cloud 107

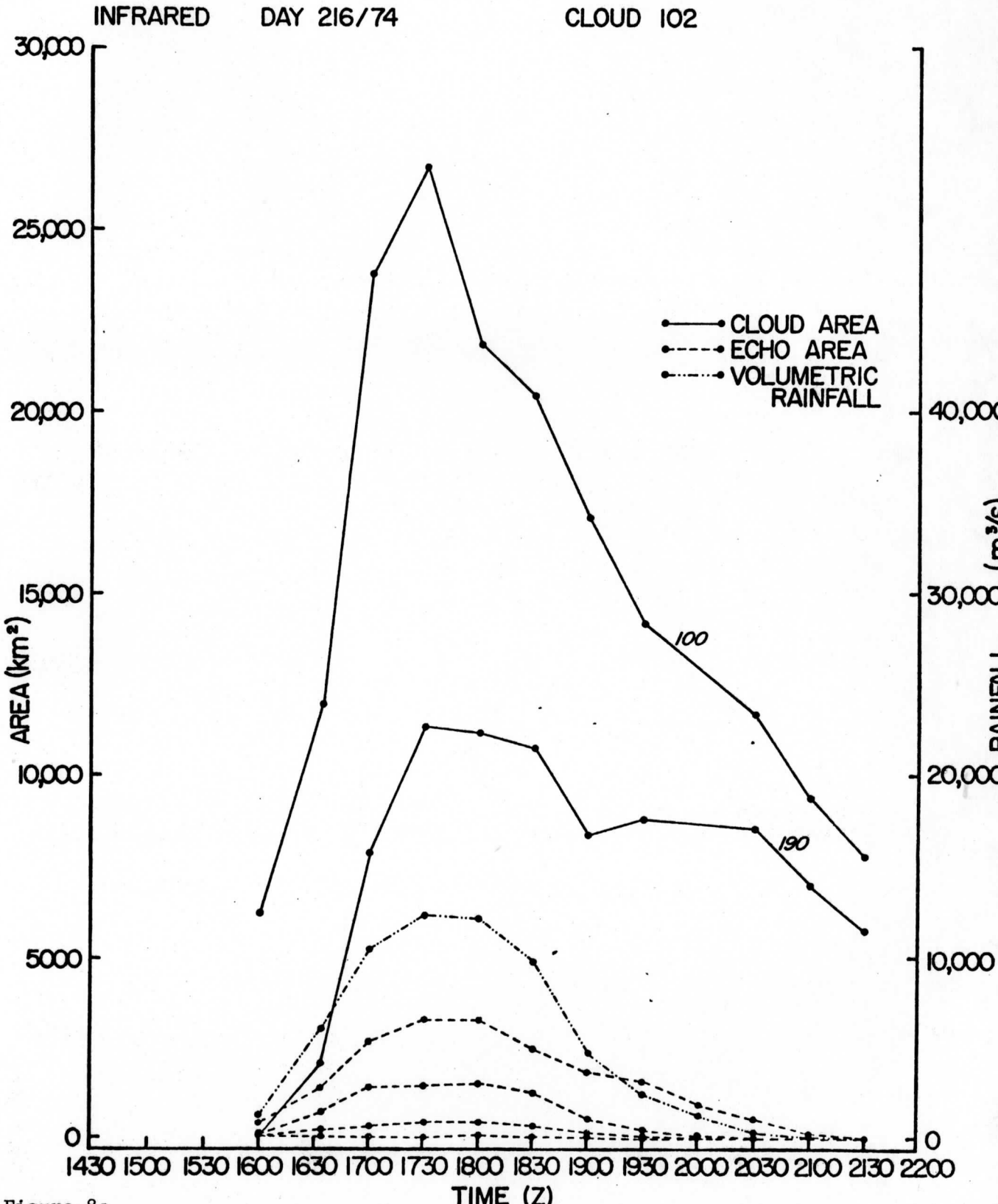

Figure 8a

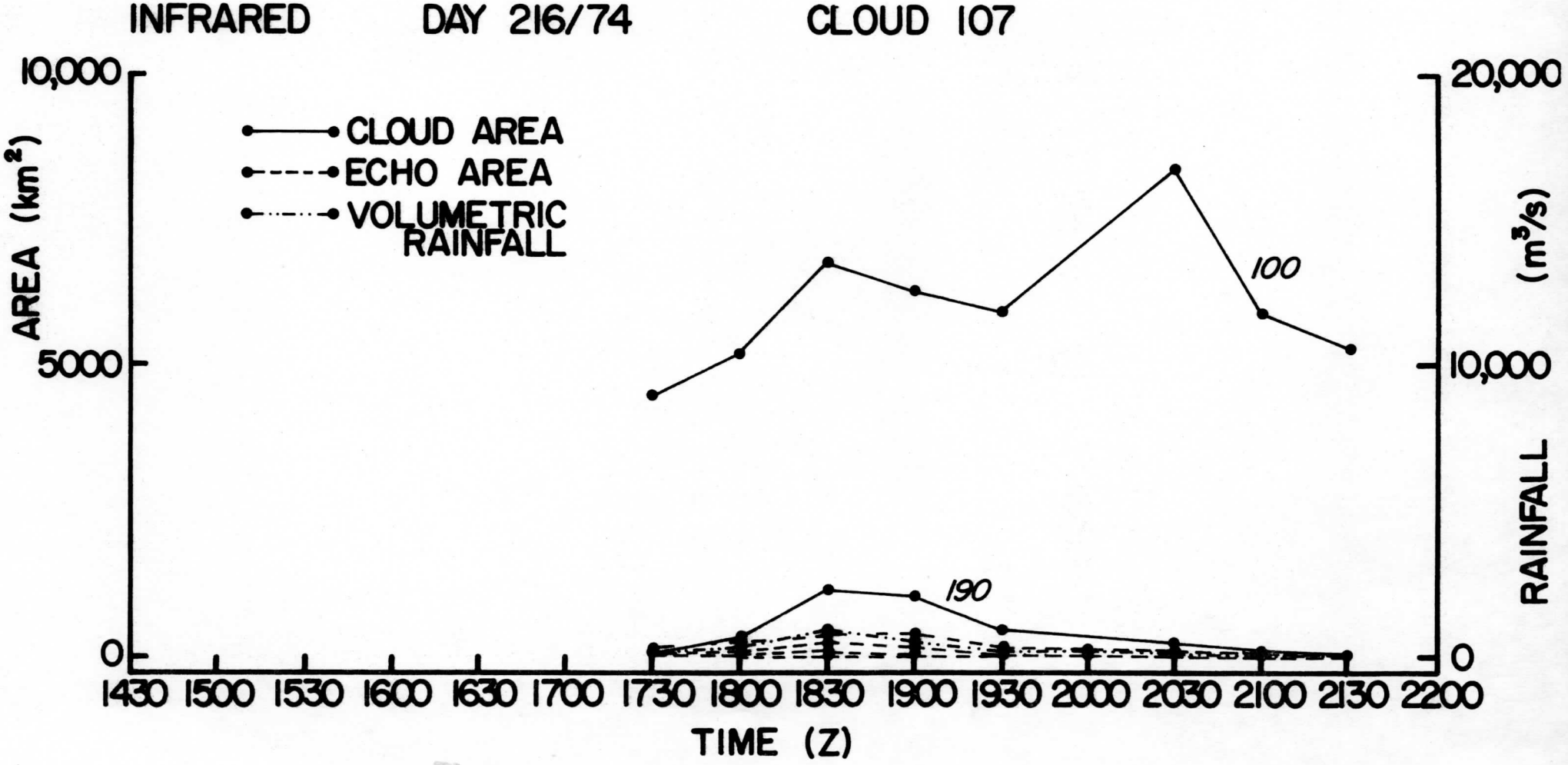
INFRARED
DAY 216/74
CLOUD 107
10,000
5000
0
AREA (km²)
CLOUD AREA
ECHO AREA
VOLUMETRIC RAINFALL
100
190
20,000
10,000
0
RAINFALL (m³/s)
1430 1500 1530 1600 1630 1700 1730 1800 1830 1900 1930 2000 2030 2100 2130 2200
TIME (Z)

Figure 8b

Figure 9 Histories of two south Florida clouds followed in SMS-1 infrared images from 5 September 1974. See Figure 6 for further information.
a. Cloud 105
b. Cloud 121

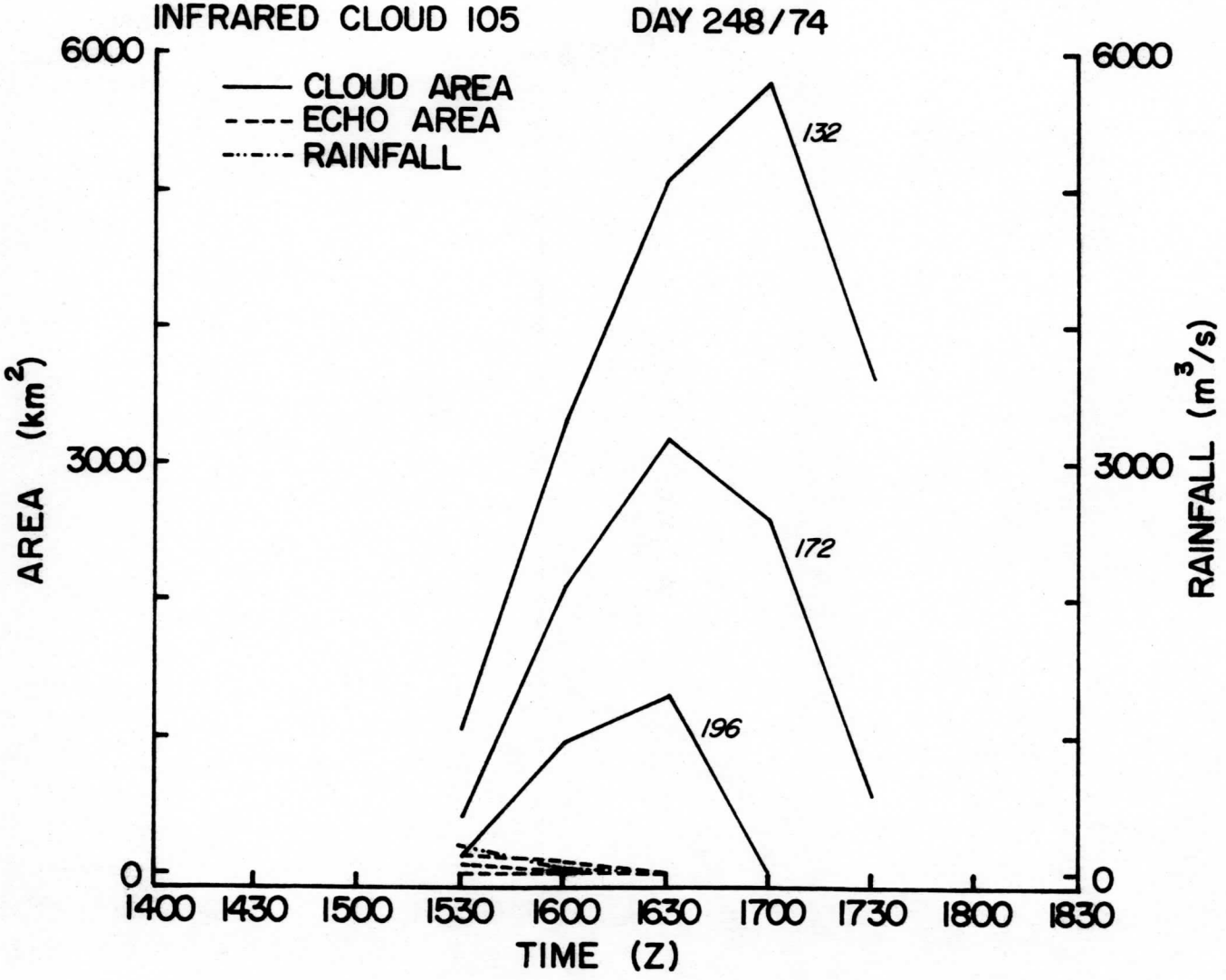

Figure 9a

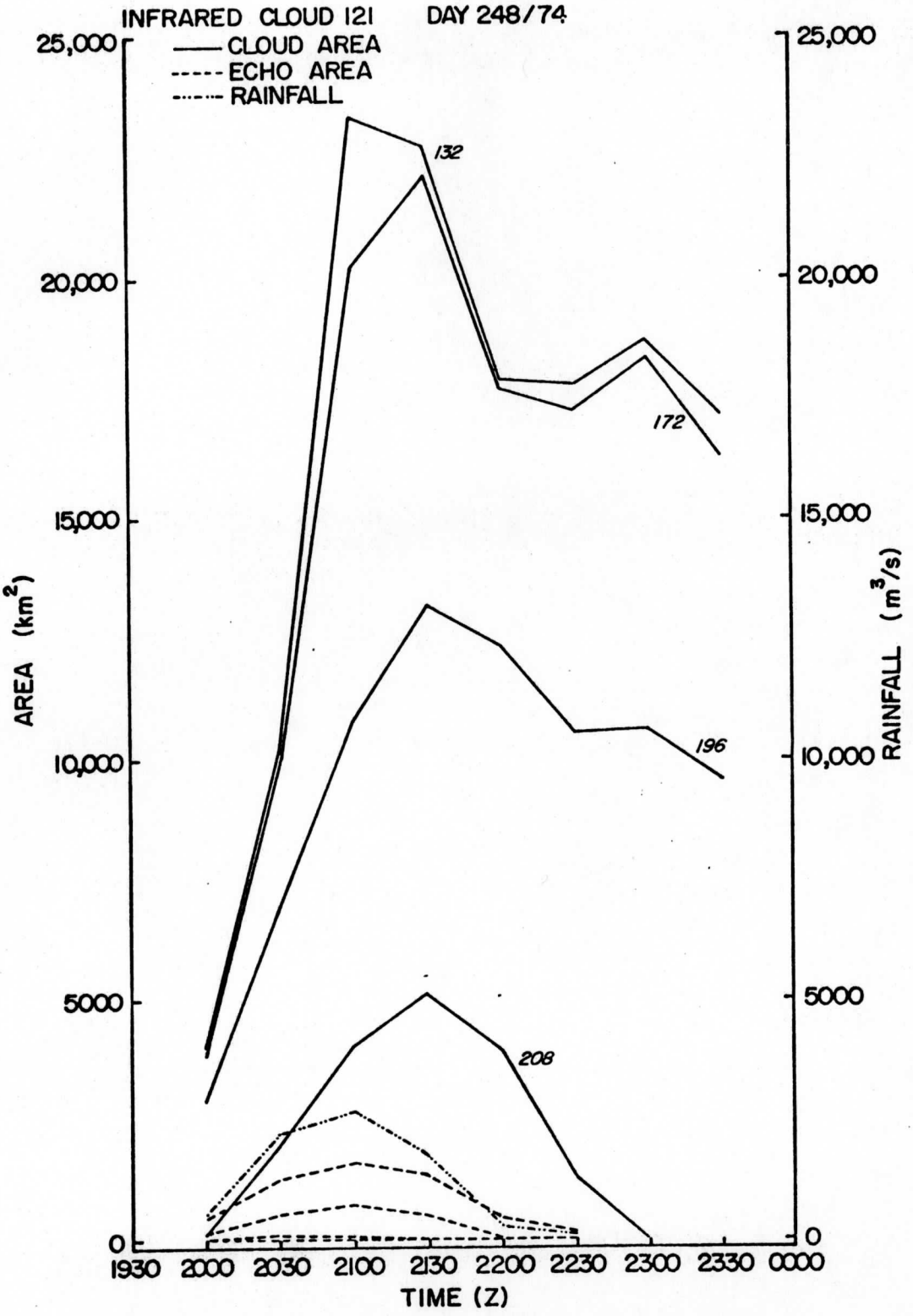
INFRARED CLOUD 121 DAY 248/74
CLOUD AREA
ECHO AREA
RAINFALL
132
172
196
208
AREA (km²)
RAINFALL (m³/s)
25,000
20,000
15,000
10,000
5000
0
1930 2000 2030 2100 2130 2200 2230 2300 2330 0000
TIME (Z)

Figure 9b

Figure 10 Histories of two south Florida clouds followed separately in SMS-1 visible and infrared images.
a. Cloud 10, 19 (visible),104 (infrared); 4 August 1974
b. Cloud 6, 106; 5 September 1974

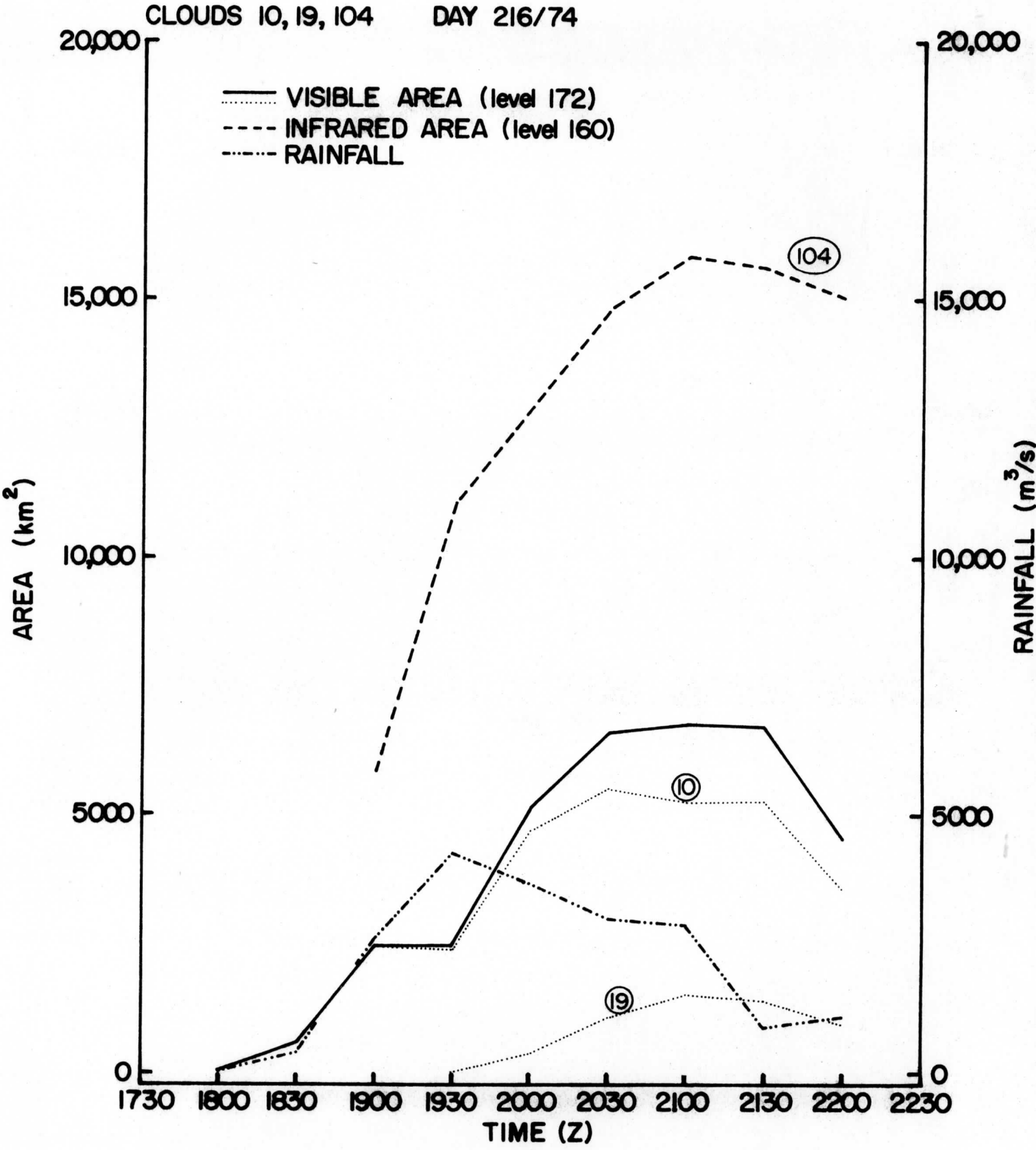

Figure 10a

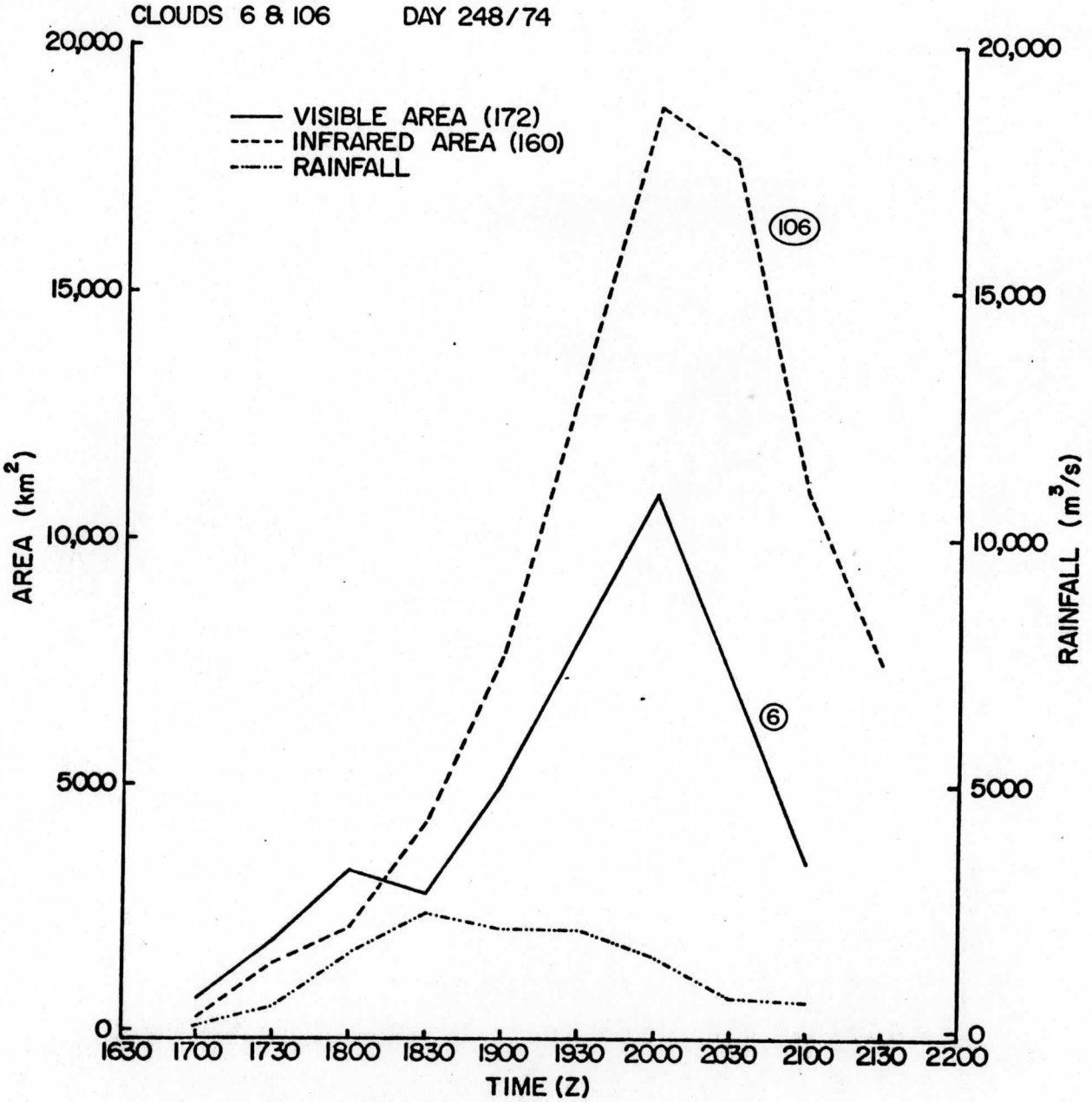
CLOUDS 6 & 106 DAY 248/74
VISIBLE AREA (172)
INFRARED AREA (160)
RAINFALL
106
6
AREA (km²)
RAINFALL (m³/s)
20,000
15,000
10,000
5000
0
1630 1700 1730 1800 1830 1900 1930 2000 2030 2100 2130 2200
TIME (Z)

Figure 10b

Figure 11 Cloud area-rainfall diagrams for clouds followed in visible SMS images. Cloud area (A_c) and volumetric rainfall (V) are normalized by maximum cloud area (A_c max). Time is implicit, increasing left to right, along the normalized cloud area coordinate. Individual clouds are represented on such a diagram by a series of points. The only clouds excluded from consideration are those for which the area maximum at 172 digital counts occurs as the first or last point on the plot.

a. 4 August 1974

b. 5 September 1974

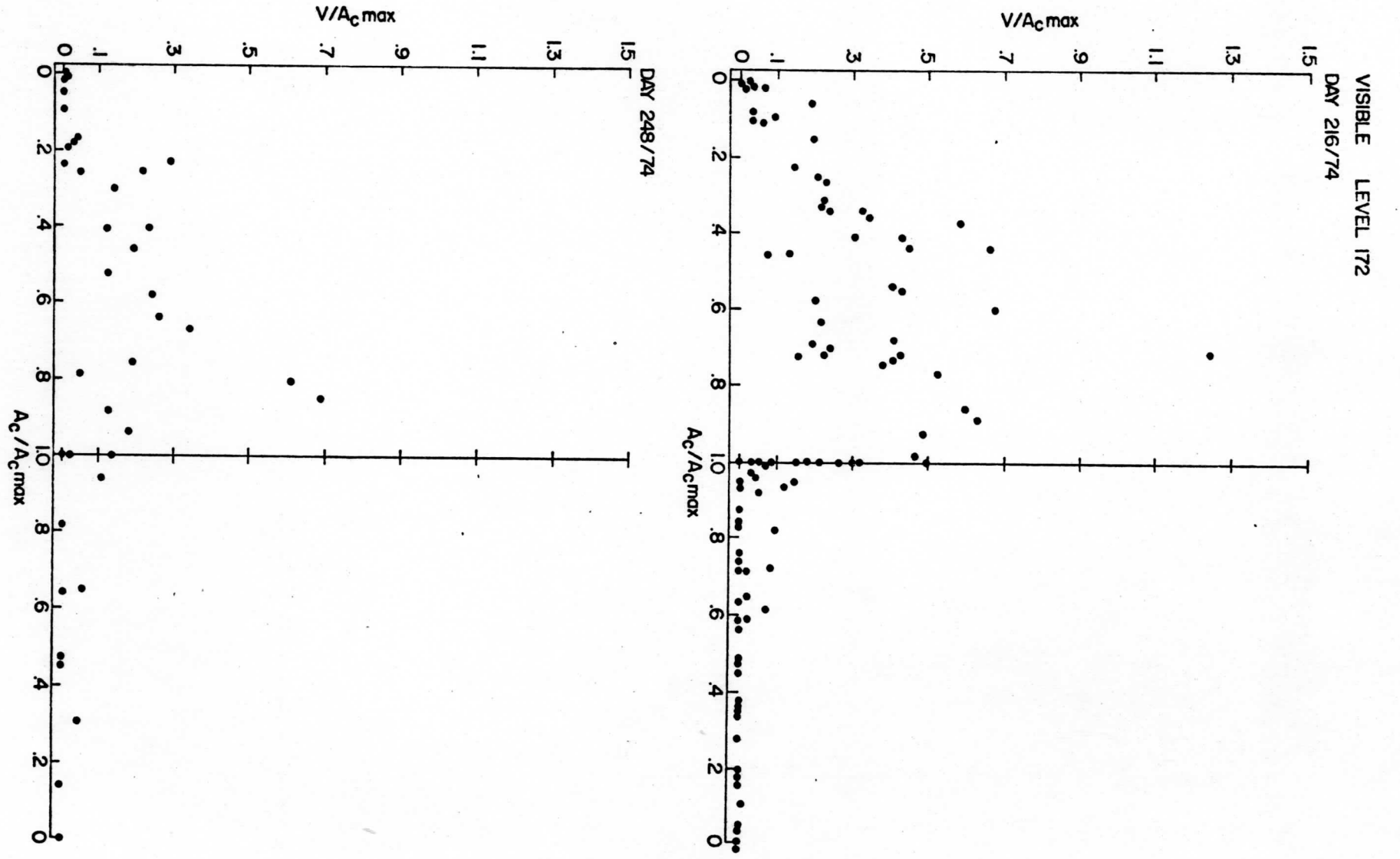

Figure 12 Cloud area-rainfall diagrams for clouds followed in infrared SMS images. Clouds are defined by the 160 digital count contour. For further information see Figure 11.
a. 5 September 1974
b. 4 August 1974

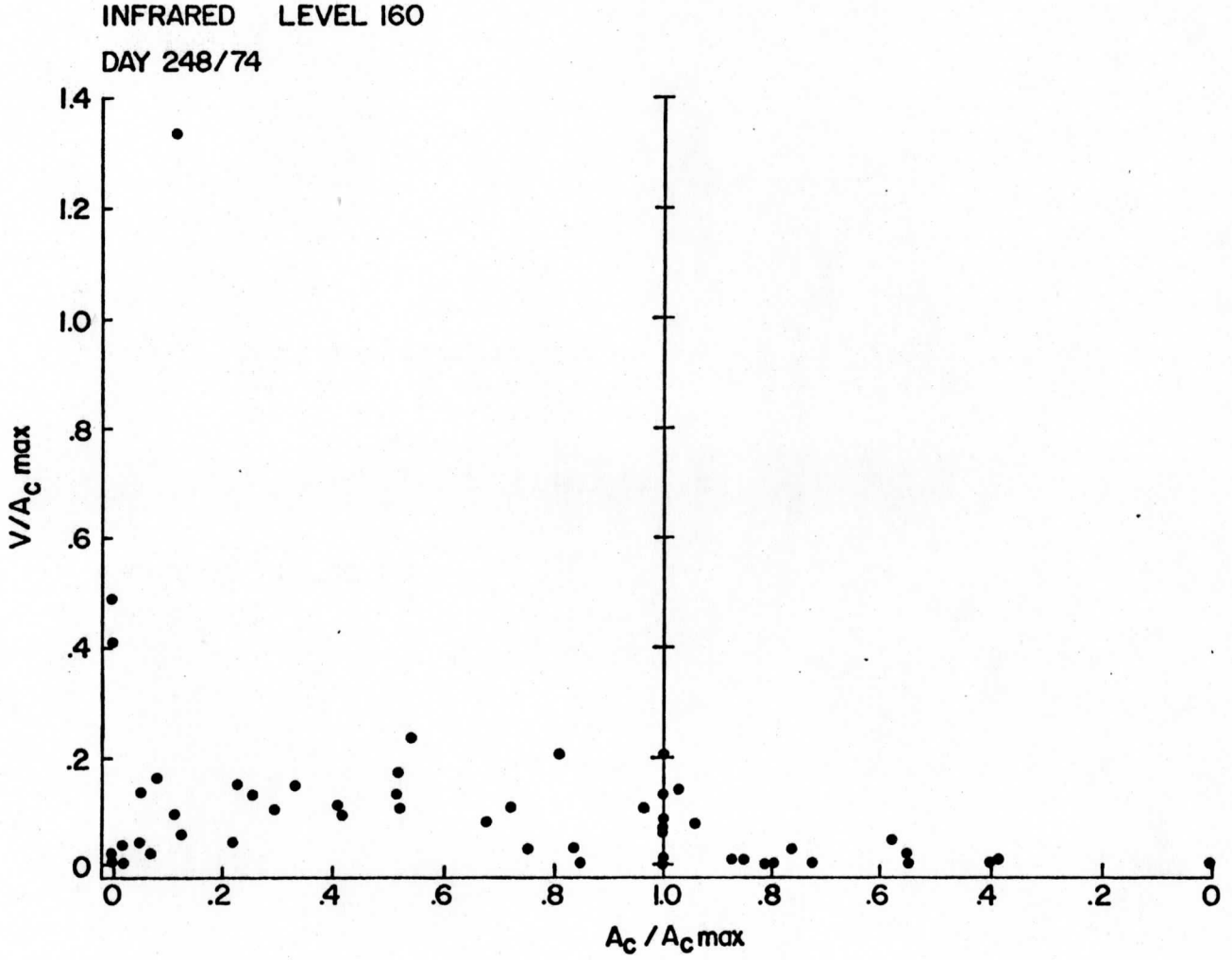

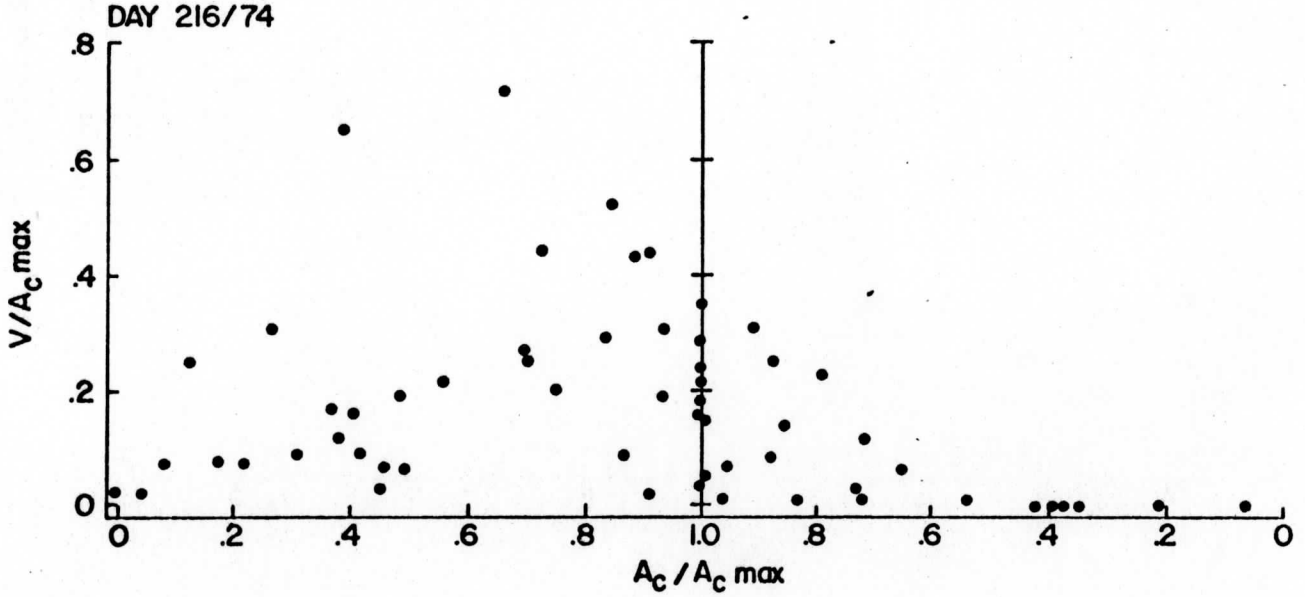

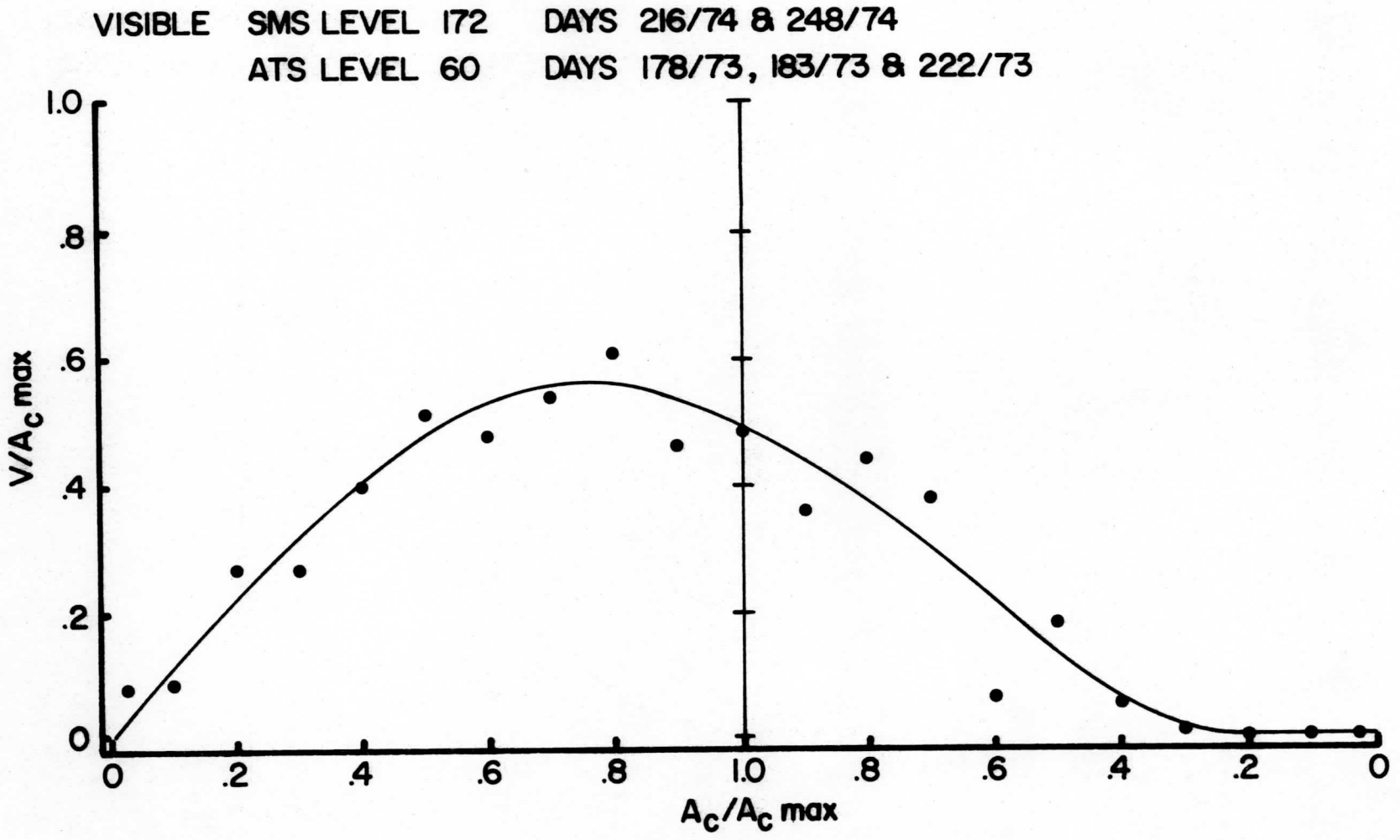

Figure 13 Averaged cloud area-rainfall diagram for ATS and SMS visible images. Clouds are defined in ATS by the 60 and SMS by the 172 digital count contour. ATS clouds with maximum brightness less than 160 digital counts were excluded, as well as clouds from both satellites whose area maximum occurs on the first or last time. For further information see Figure 11.

APPENDIX A

ATS-3 Calibration

The procedure described in the Equivalence Section gives a relationship between normalized ATS-3 and SMS-1 brightness levels for three particular days in 1974. To extend this relationship to 1973 ATS, it must be shown that the ATS signal strength was the same in 1973 and on these days in 1974. Calibration of the ATS-3 sensor, which is described more fully in Appendix B Section IID, requires selection of a very bright cloud. The ratio of theoretical brightness for a model bright cloud at this location to measured brightness of the actual cloud is the calibration factor, alpha.

One source of variation in alpha is caused by line to line signal fluctuations. In 1973 ATS data, some lines were brighter than their neighbors over the width of a cloud. To use measured brightness from such a line would give an artificially low alpha. Deciding when a line falls in this category and when it should be avoided introduces some subjectivity. Another source of variability in alpha results from selected clouds not all being of model optical thickness, which has a brightness of 3% below the limiting brightnes value and corresponds to a geometric thickness of 14 km or 40,000 ft. Since clouds do approach a limiting brightness (see Appendix B), one would expect a clustering on the low end of the alpha range. The actual variation of alphas is shown for the 1974 days in Figure 14.

The first alpha measured from 1973 data gave a value of 19 for day 222 for a small sample. Data from other days subsequently showed 18 was a better value and that was taken as the best value for 1973 days. In 1974, a value of 17 was found for each of three days, and 21 for a fourth day. Considering typical scatter in alpha measurements, 18 and 17 are essentially the same value, but an alpha of 21 is definitely a change.

Thus we conclude that the ATS-3 signal strength remained essentially constant from the beginning of summer 1973 until shortly before 5 September 1974 when it dropped.

Is it legitimate to combine 222/1973 data with the rest of our 1973 ATS-3 and 1974 SMS-1 data since an alpha of 19 was used for its normalization? To answer this, a normalization was done from our lowest sun angle (at 1430 Z) to our ATS reference point with alphas of 17 and 19. Then from the brightness vs. area graph of a typical cloud, the error in area was calculated and plotted in Figure 15. For the brightness level utilized in our size normalized rain volume-cloud area diagrams used in rain prediction, the error was 2%. The error was 8% or less for all but our highest level we measure, and that level's error was 25%.

Figure 14 Calibration factor, alpha, as a function of time. Signal was essentially constant until the last day in 1974.

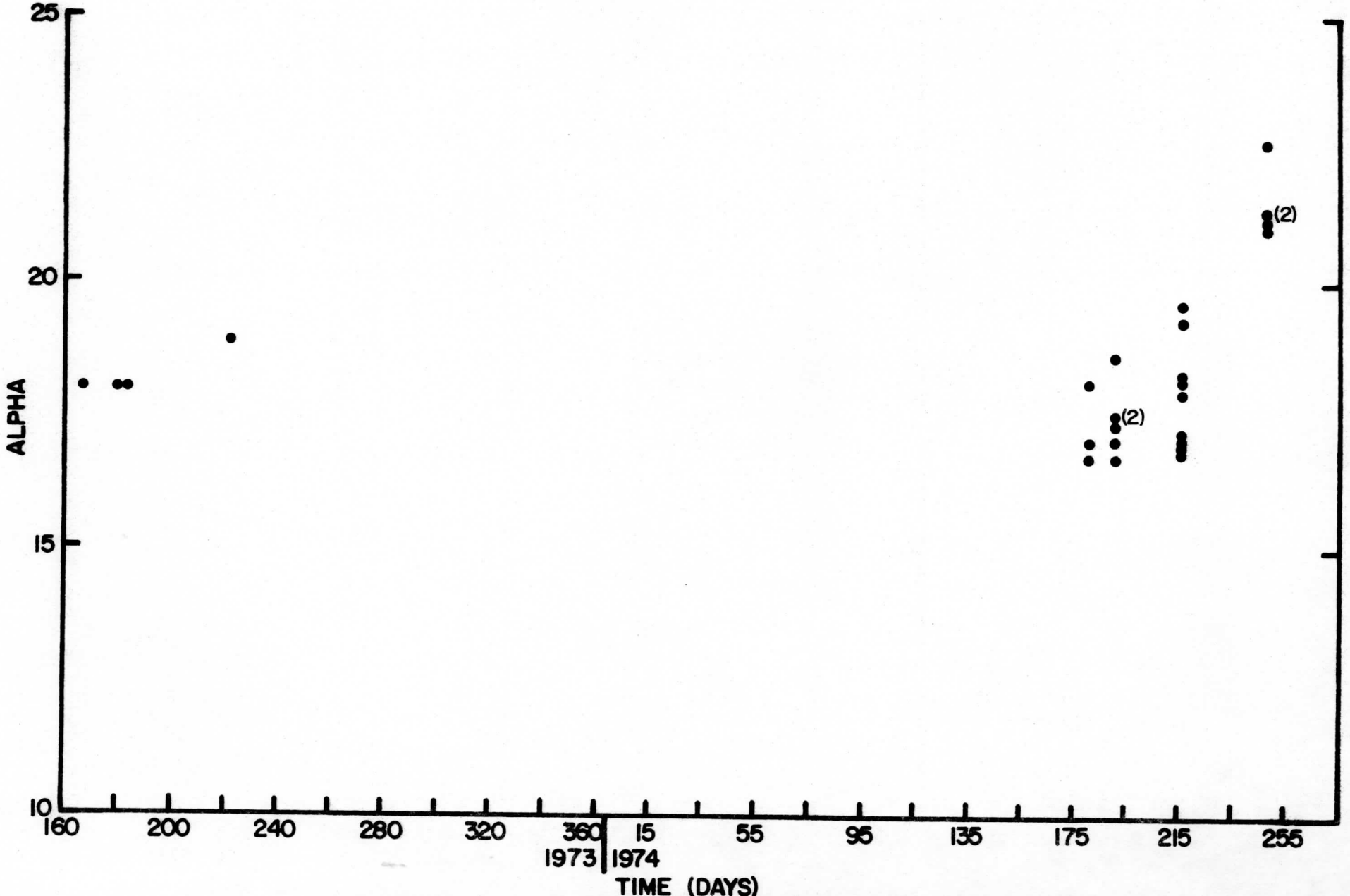

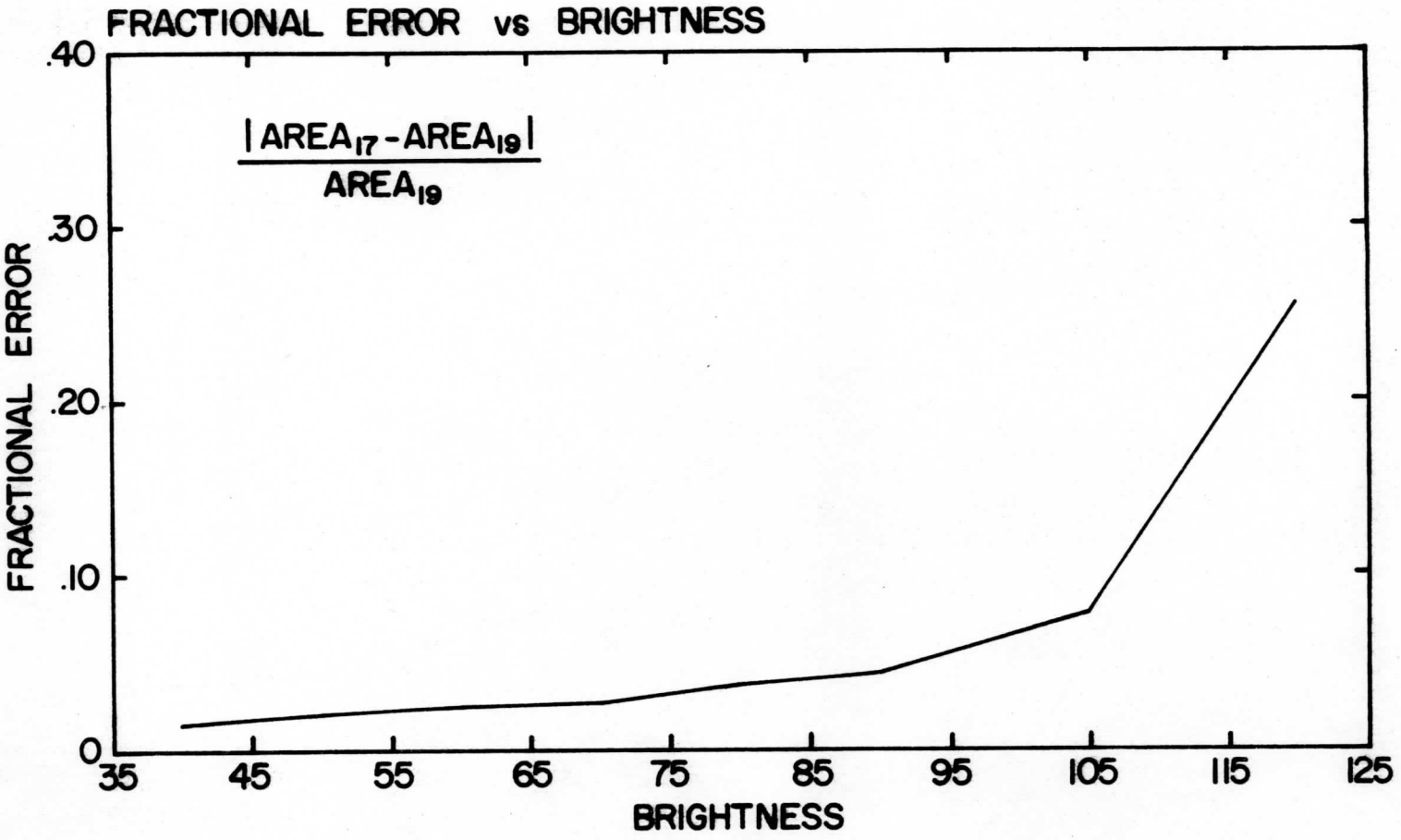

Figure 15 Magnitude of area error from using an alpha of 19 instead of 17 for a typical cloud on day 222/73. Brightness levels were normalized from the time of the largest sun angle (1430 Z) to the ATS reference point using one alpha and then another. Then from a brightness vs. area graph of a typical cloud, the area error was calculated.

APPENDIX B

BRIGHTNESS NORMALIZATION OF SATELLITE IMAGES

by Frederick Mosher

I. INTRODUCTION

Brightness normalization is removal of the effects of changing angles of illumination on observations of satellite images. Meteorological satellites such as the SMS/GOES and others presently provide high resolution visible images of the earth on a routine basis. These images provide the coverage and resolution necessary for quantitative measurements of convection and properties associated with convection such as rainfall estimation. However, quantitative analysis methods which use the brightness of the cloud in the measurements are faced with the problem that as the sun changes its position, the changing angle of illumination causes a brightness change of the clouds in the image. This brightness change caused by the sun's movement must be removed so that brightness changes caused by convective growth or decay can be accurately measured. The problem of brightness normalization was addressed in the workshop on Meteorology of the Near Future Prospects of Image Pattern Recognition sponsored by the National Science Foundation on 11 November 1974. The final report of the workshop states:

> "The effect of the angle of illumination on observations is fairly well understood from a theoretical point of view. The effects of this on the observations from space are not adequately considered. The removal of this effect from the observed data is a complex and involved procedure. As the science evolves the effect will have to be removed to permit a clearer study of the underlying meteorologic phenomena. It should also be possible to obtain some information from shadow effects when they are known. The committee felt that it will be necessary to find a way to remove the illumination effect in the very near future."

II. SCATTERING FROM CLOUDS

The light received by the satellite has been scattered by the droplets in the clouds. The visible light scattered by clouds depends upon several

variables:

a. The droplet size distribution and shape of the cloud particles

b. The number density of the scattering particles in the cloud

c. The cloud thickness

d. The angular conditions of the measurement system (the zenith angles of the sun and the sensor, and their relative azimuth angle)

e. The shape of the cloud.

A. Normalization Procedures

In quantitative studies of convective cloud growth ideally only one of the variables should change at a time. The normalization procedure should correct for all the changes of the variables except the one which is under study. However since information on the states of all the variables is generally not available at the satellite, some of the variable effects must be parameterized in any normalization technique.

There have been several approaches to parameterizing the variables of the cloud scattering problem in the development of normalization procedures. The simplest approach has been to neglect all the cloud variables and assume that the clouds are perfect isotropic reflectors and obey Lambert's law. The intensity of the reflected light will vary as the cosine of the solar zenith angle for an unchanging cloud. Martin and Suomi (1972) have shown that the tops of cumulonimbus clouds display a Lambertian behavior, and a cosine correction can be used to normalize the brightness of thick cumulonimbus clouds.

There is, however, considerable evidence in the literature that neglecting all the variables and assuming isotropic reflectance can lead to erroneous results. Bartman (1967), Ruff et al. (1968), and Brennan and Bandeen (1970) have experimentally measured the scattering from clouds.

They found clouds generally show an anisotropic reflectance pattern which varies with solar zenith angle. Normalization procedures based on this empirical data base have been developed by Sikula and Vonder Haar (1972). The main problem with this type of normalization has been the limited amount of empirical data available. Since empirical data on the variation of the reflectance pattern which is caused by variations in cloud thickness is generally not available, the normalization procedures based on empirical data generally have neglected the effects of cloud thickness. Studies by Mosher (1974) have shown that different thicknesses of clouds will require different normalization corrections. The brightness contrast in a cloud was shown to vary as a function of the scattering geometry, implying that different thicknesses of clouds scatter light differently.

To overcome the limitations imposed by a restrictive data base, the normalization procedure which has been developed in this study makes use of a theoretical multiple scattering model to generate a large data base for a large number of possible sun and observation angles. Data was generated for 16 different thicknesses of clouds.

B. Multiple Scattering Model

The multiple scattering program which was used to generate the data base of cloud reflectance patterns was a doubling method model developed by James Hansen of NASA's Goddard Institute for Space Studies. The details of the model are published in the January 1971 issue of the Journal of Atmospheric Sciences. Results from the model are published in the November 1971 issue of JAS (Hansen, 1971, a, b).

The doubling method works for a plane-parallel homogeneous cloud. Numerical computations begin with a layer of such small optical thickness that scattering and transmission can be described by single scattering theory. The cloud thickness is built up by putting two layers together and

computing the interactions that take place. The process of taking two layers, computing the transmission, reflection and interaction, combining the two into a single layer and then repeating the process for the new layer is the "doubling" procedure. By doubling, the thickness of the cloud increases by a factor of two after each computation, so very thick clouds can be generated quickly on the computer.

The single scattering phase function used as input to the multiple scattering doubling program was Deirmendjian's C-1 cloud model phase function. The forward scattering peak of the phase function was truncated and spread by the multiple scattering model (Hansen and Pollack, 1970). Conservative scattering was used with the local single scatter albedo set to unity.

The multiple scattering model as originally configured had the surface under the cloud as a perfectly absorbing black surface not accepting any other lower surface. While land and sea surfaces are dark compared to cloud, they are not entirely negligible, particularly for thin clouds. In order to include the sea surface brightness, the assumption was made that the light reflected from the sea was small compared to the light reflected from the thicker clouds, so that the energy which was lost by the light coming from the sea through the cloud toward the satellite did not interact with the light scattered originally in the cloud. The cloud scattering and the sea surface reflectance were computed separately and the results added.

The sea surface brightness was computed using sea surface albedo values from Payne (1972). Payne performed an extensive experimental study of the albedo of the sea surface from a fixed platform and published tables of sea surface albedo as a function of the sun's altitude and atmospheric transmittance. To use these tables, the downward flux through the clouds

and the atmospheric transmittance was computed. The flux impinging on the sea surface was then multiplied by the approximate albedo value to give a value for the flux propagating upwards from the sea surface. This upward flux was used as a new source of radiation and the directional transmittance to the satellite was computed using the multiple scattering program. The intensity of the sea surface was then added to the intensity of the cloud. Figure 1 shows the graph of intensity versus optical thickness with and without the sea surface brightness. As can be seen from the graph, the effect is significant for thin clouds.

The Rayleigh scattering of the atmosphere has been neglected in these calculations because its effect is smaller than the other effects. The sea surface brightness, as seen in Figure 1, is approximately .08. The brightness due to Rayleigh scattering for this geometry is .018, a factor of four less.

C. Parameterization of Variables

The amount of light scattered from real clouds depends upon the droplet size distribution of the cloud, the number density of scatters, the cloud thickness, the angular geometry of the sun and sensor, and the finite shape of the cloud. Some of these variables can be measured and used in the normalization, but others must be parameterized.

The physical thickness and the number density of the droplets can be combined into the single variable of optical thickness:

$$\tau = KZ; \quad K = \sigma\rho$$

τ = optical thickness

Z = physical thickness

K = extinction coefficient

σ = scattering cross section

ρ = number density of scatters

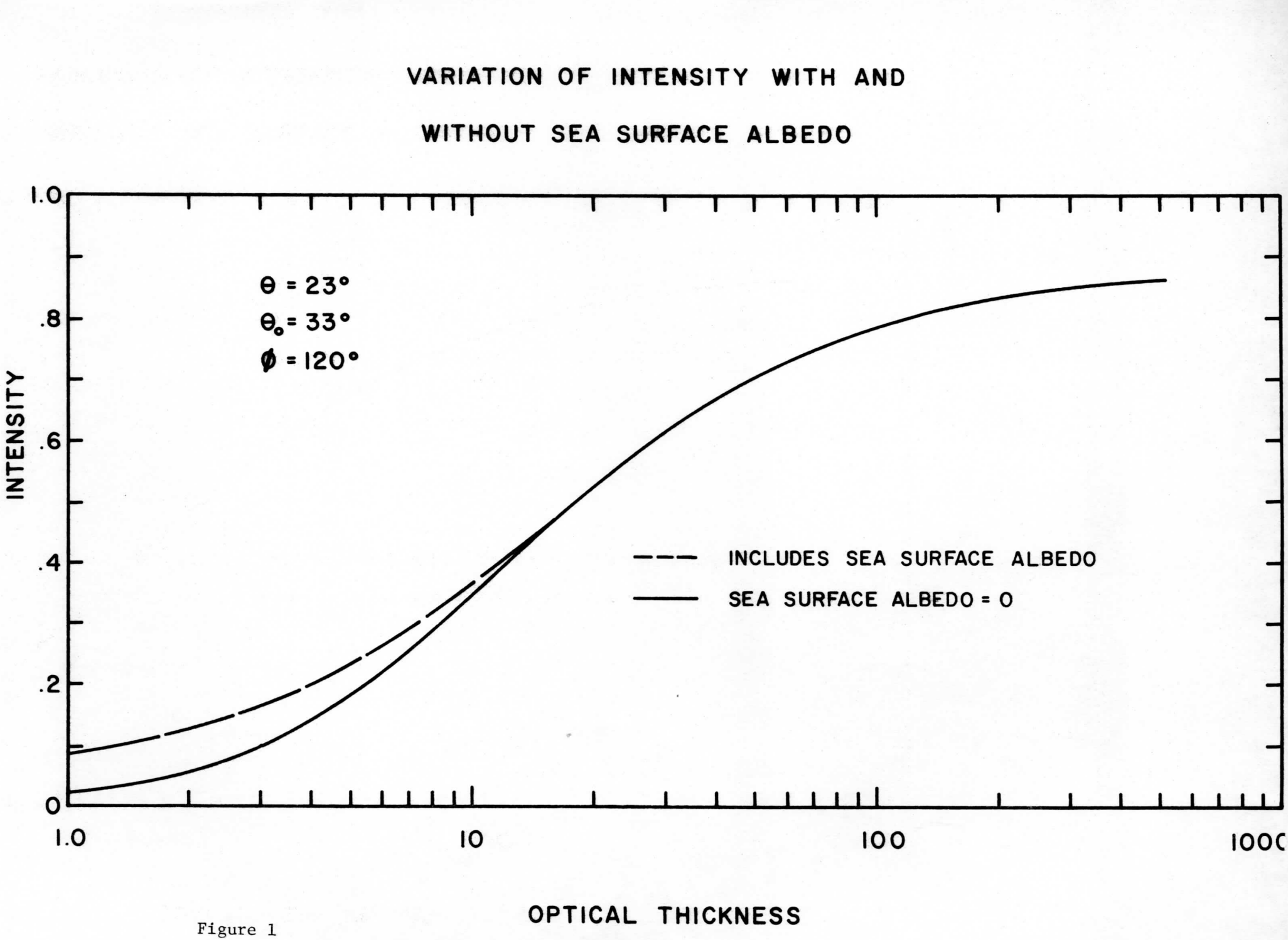
VARIATION OF INTENSITY WITH AND
WITHOUT SEA SURFACE ALBEDO
1.0
.8
.6
.4
.2
0
INTENSITY
θ = 23°
θ₀ = 33°
ϕ = 120°
INCLUDES SEA SURFACE ALBEDO
SEA SURFACE ALBEDO = 0
1.0
10
100
1000
OPTICAL THICKNESS

Figure 1

The optical thickness τ of a layer is such that unit radiation normally incident upon the layer is reduced by single scattering in passing through to $e^{-\tau}$. The optical thickness, rather than the physical thickness, has been used in all the multiple scattering calculations since it combines the effects of the variables of number density and scattering cross sectional area.

The effect of variations in the particle size distribution on the intensity of light reflected from clouds is minor. The wavelength of the light is on the order of .5 microns. The particle size distribution of clouds have radii on the order of 5 to 10 microns (Diem, 1948). The droplets are very large compared to the wavelength of the light being scattered. The single scatter phase function has a very large forward scatter peak. Hansen (1971b) has shown in the near infrared that variations in the size of the particles do not greatly influence the multiple scattering intensities when the particles are large compared to the wavelength of the light. Figure 2 shows for visible light the variations caused by differences in the particle size distribution for 4, 7, and 10 micron average radius particles. The phase functions for these particle distributions were generated by a Mie scattering program developed by James Hansen, NASA/GISS. The particle size distributions of each had a variance of .111. The particle size distribution used was a variation of the gamma distribution (Hansen, 1971b). The vertical axis in Figure 2 is intensity in theoretical units for an input flux of π, while the horizontal axis is optical thickness. The sun and the sensor both had a zenith angle of 0°. A 12 micron average radius particle size distribution was also computed, but its curve for Figure 2 was indistinguishable from the 10 micron curve. Consequently, for this study the variation of intensities of scattered light caused by variations in the particle size distribution has been neglected. The 4 micron average radius distribution of Diermendjian was chosen to represent all clouds

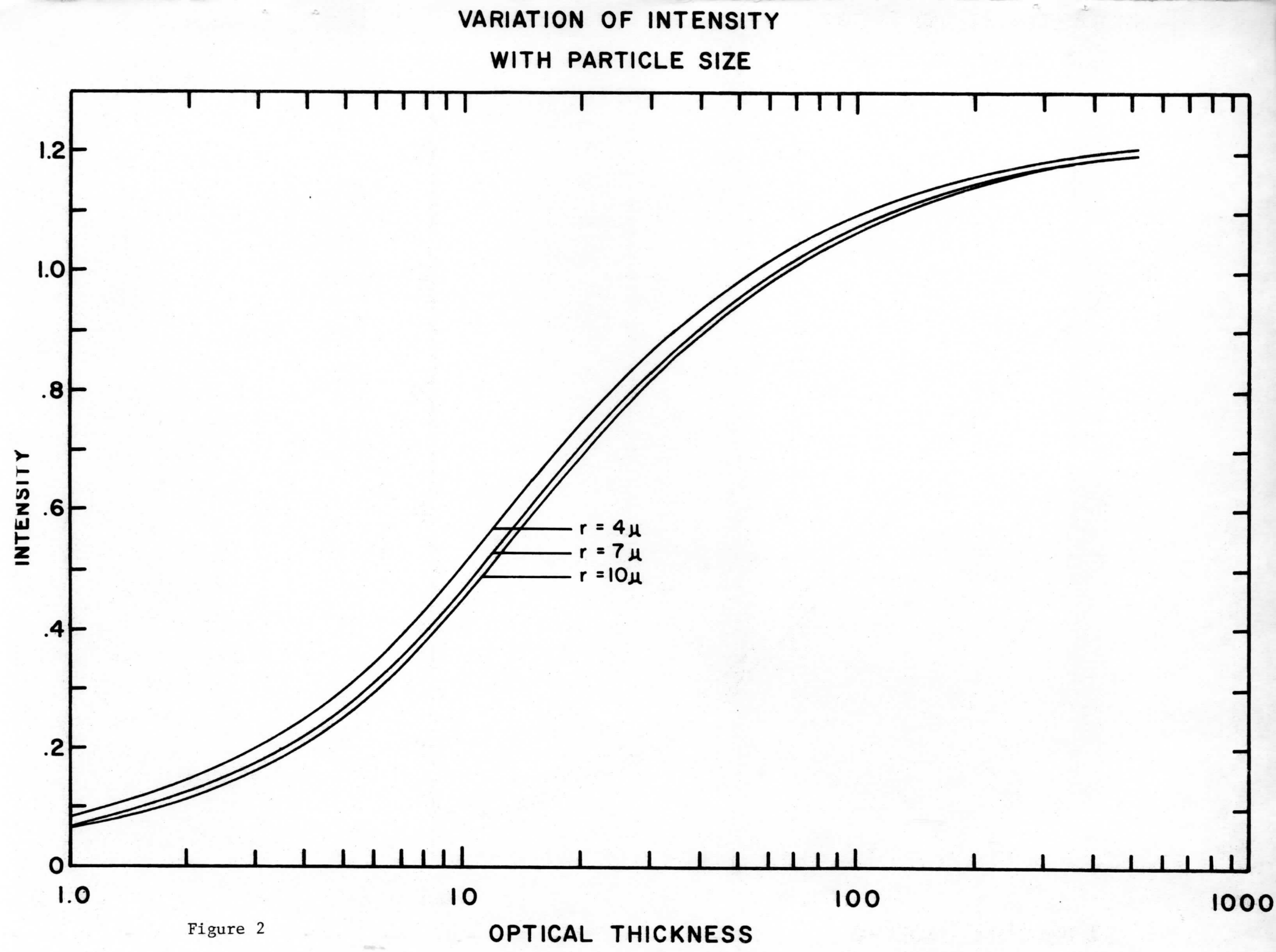
VARIATION OF INTENSITY
WITH PARTICLE SIZE
INTENSITY
1.2
1.0
.8
.6
.4
.2
0
r = 4μ
r = 7μ
r = 10μ
1.0
10
100
1000
OPTICAL THICKNESS

Figure 2

satellite, and the position of the sun. Since a wind measurement using cloud tracers already requires an accurate navigation of the satellite, the information required to calculate the angle of the measurement is readily at hand.

In determining the scattered intensity of the cloud, the variables have been reduced to optical thickness and angles. The effects of particle size distribution are small and the effects of finite size of clouds have been neglected. The determination of cloud thickness, and the implied normalization which takes place, can be performed by taking the intensity measurement from a calibrated satellite and converting it to optical thickness through use of the tables of intensity versus optical thickness generated by the multiple scattering program.

D. Calibration of the Satellite Sensor

Although controls on signal level are better for SMS/GOES than for the early Applications Technology Satellites (ATS), in performing quantitative radiance calculations, such as determination of cloud thickness, there still is a need for calibrating the satellite. In order to calibrate a satellite in orbit, a landmark of known brightness must be found. Previous attempts at calibration include using the moon (Hanson and Suomi, 1968), White Sands, and the South American salt flat Salar de Uyuni (Griffith and Woodley, 1973). Calibrations using these landmarks have been hampered by the lack of detailed knowledge of the bi-directional reflectivity characteristics of these landmarks.

This study has taken a different approach at calibration of satellite images. Figure 3 shows an example of intensity versus optical thickness for the case of a solar zenith angle of 35°, satellite zenith angle of 20°, and relative azimuth angle of 50°. As can be seen from the figure as the cloud becomes very thick, the intensity starts to approach a limiting value. The

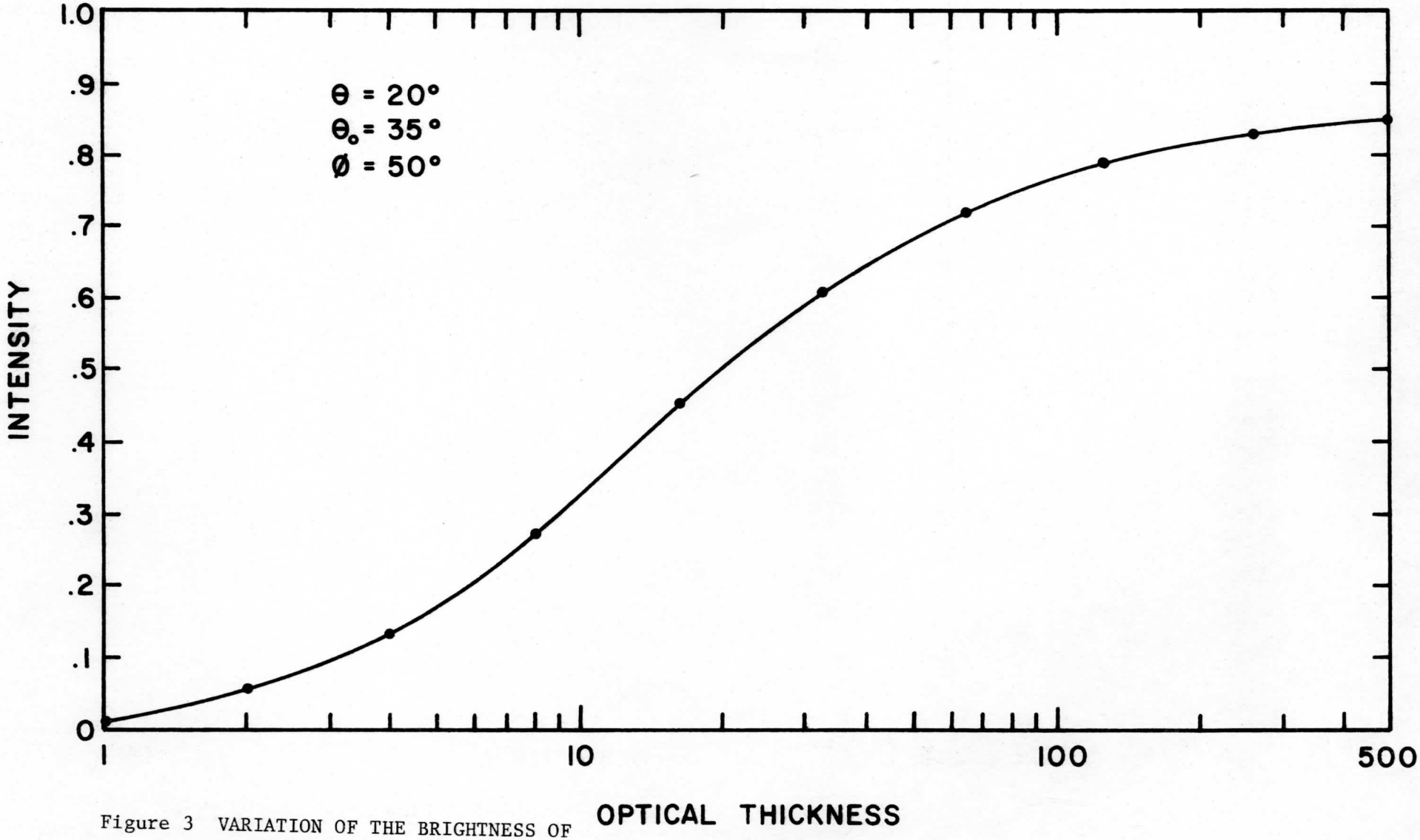

Figure 3 VARIATION OF THE BRIGHTNESS OF A PLANE PARALLEL CLOUD WITH CHANGES IN THE OPTICAL THICKNESS OF THE CLOUD

including cirrus. Cirrus should be able to be represented by this distribution since it appears that as the particle sizes increase over 10 microns, no appreciable change in the reflected intensity occurs.

The effects of the finite shape of the clouds is largely unknown. The plane-parallel cloud which was used in the theoretical multiple-scattering doubling program had no horizontal limits. Experimental measurements of scattering from clouds such as Bartman (1967) and Brennan and Bandeen (1970) generally use stratus type clouds which also have no horizontal limits. For clouds with vertical extent approximately equal to their horizontal extent, such as cumulus clouds, some light energy should be lost or gained through the sides in addition to what comes through the top and bottoms. McKee and Cox (1974) have performed a study on the effects of the finite shaped clouds by using a Monte Carlo multiple scattering program on a cube. The angular resolution of their study was limited to light leaving the top, side, and bottom of the cube. Their results show that the upward reflected light from the cube is about 25% less than for the semi-infinite cloud. However, their angular resolution was not sufficient to distinguish between the intensity of light coming from the top center and the intensity coming from the top edges. One would expect more light to escape from the edges than from the middle and a gradient of brightness should be established due to the light escaping out the sides. Unfortunately, there is presently no data avaiable on this problem. Consequently, for this study, the intensities from the doubling program, which uses a semi-infinite horizontal extent cloud, will be used. There will be some errors at the edges of the clouds, but hopefully the errors at the centers of the clouds will be small.

The variable parameter of the angles of the sun and the sensor can easily be calculated with the knowledge of the position of the cloud, position of the

fact that clouds become intensity saturated and reach a limiting value has been the basis for a satellite calibration technique. Using the multiple scattering program, it was determined that the optical thickness 512 has a brightness which is within 3% of the ultimate limiting brightness. A cloud with optical thickness 512, droplets of 10 micron diameter, and droplet density of 250 droplets/cm^3 (as is representative of a heavy convective cloud) would have a physical thickness on the order of 14 km or 40,000 feet. Consequently, if edge effects can be neglected, any well-developed thunderstorm or tropical cloud cluster should have an intensity within 3% of the brightness of an infinitely thick cloud observed under the same sun and satellite angles. Small variations in the physical thickness should not make much difference in the brightness of these very thick clouds.

The calibration procedure used in this study involved selecting a very bright thick cloud and assigning it an optical thickness of 512. The ratio of the theoretical intensity of a cloud of optical thickness 512 to the measured intensity of the very thick cloud was designated the calibration factor alpha (α). With this calibration factor, any measured intensity can be converted into theoretical units by multiplying it by alpha.

III. BRIGHTNESS NORMALIZATION PROGRAM

By use of the data generated by the multiple scattering program, measured intensities of clouds can be converted into optical thickness. The parameter optical thickness is independent of sun and satellite angles, and as such, it is a normalized parameter. To convert to a normalized brightness, the optical thickness can be converted back to intensity for a standard sun, satellite geometry.

A. Segmenting the Image

Satellite images, such as the SMS and ATS images which have been used

in the normalization studies, have a very high resolution so that there are a very large number of pixels in each image. If each image pixel were to be handled separately, and new normalization information were to be calculated for each pixel, the computer time would become excessive. To get around this problem, the normalization program segments the image into boxes no larger than 1° of latitude square. The assumption is made that the zenith angles of the sun and satellite are constant over this segmented box. Hence a conversion table of brightness to optical thickness can be computed at the center of the box, and this table can than be applied to all the pixels within the box.

B. Method of Computing Optical Thickness

The optical thickness of a cloud is determined from the brightness of the cloud. A multiple scattering program using the doubling method developed by James Hansen of NASA/GISS was used as the source of data for the conversion between brightness and optical thickness. Since the McIDAS Datacraft computer used in the brightness normalization processing is too small to run the multiple scattering program, a large table of 77,824 intensities was generated on the University of Wisconsin's UNIVAC 1110 and stored on the McIDAS digital disk. This represents all possible combinations of 16 solar zenith angles, 16 satellite zenith angles, 19 relative azimuth angles, and 16 optical thicknesses. The received SMS visible data has a six bit word with a square root digitization. In order to deal with a linear brightness scale, the SMS data is squared, causing a 12 bit word. The large table of intensities has been multiplied by a scaling factor of 3166.9 prior to storage so that a 12 bit integer word which matches the SMS intensity resolution can be achieved. Other satellites, such as the ATS, which have a linear digitization with less than a 12 bit word can use the tables directly.

The normalization program first determines the solar zenith angle, satellite zenith angle, and the relative azimuth angle for the center of the segmented box. The conversion of any visible pixel in that box from brightness to optical thickness is done by using the large table of intensities. Since the table only holds data at finite angles, an interpolation must be performed in order to obtain the optical thickness for a unique set of input angles. The program first generates a table of 16 intensities for 16 standard optical thicknesses by doing a linear interpolation from data on the digital disc. The intensity of any intensity I which is a function of sun angle θ_o, satellite angle θ, azimuth angle ϕ, and optical thickness τ can be determined by

$$I_{(\theta,\theta_o,\phi,\tau)} = \left(\frac{\partial I}{\partial \theta}\right)_{\theta_o,\phi,\tau} d\theta + \left(\frac{\partial I}{\partial \theta_o}\right)_{\theta,\phi,\tau} d\theta_o + \left(\frac{\partial I}{\partial \phi}\right)_{\theta_o,\theta,\tau} d\phi + \left(\frac{\partial I}{\partial \tau}\right)_{\theta,\theta_o,\phi} d\tau + I_{(\theta_1,\theta_{o_1},\phi_1,\tau_1)}$$

with $I_{(\theta_1,\theta_{o_1},\phi_1,\tau_1)}$ being known.

For a constant optical thickness the intensity I can be obtained by finite differences as

$$I_{(\theta,\theta_o,\phi)} = \frac{\Delta I}{\Delta\theta}\Big|_{\theta_o,\phi}^{(\theta-\theta_1)} + \frac{\Delta I}{\Delta\theta_o}\Big|_{\theta,\phi}^{(\theta_o-\theta_{o_1})} + \frac{\Delta I}{\Delta\theta_o}\Big|_{\theta,\theta_o}^{(\phi-\phi_1)} + I_{(\theta_1,\theta_{o_1},\phi_1)}$$

In the partial derivatives, i.e., $\left.\frac{\Delta I}{\Delta\theta}\right|_{\theta_o,\phi}$, the quantities θ_o and ϕ are held constant. Since there are only values of I at finite values of θ_{o_1} and θ_{o_2}, ϕ, and ϕ_2 available on either side of θ_o and ϕ, the finite values closest to θ and ϕ were chosen for the derivatives. The calibration factor of the visible sensor is then used to convert the observed brightness into the same units as the intensities on the digital disk. Then a linear interpolation is performed on the table of 16 intensities for 16 standard optical thicknesses to convert the observed brightness into optical thickness.

However, when the calibration factor α has been determined by using thick convective clouds, as just described, there exists a possibility that the finite size of the cloud affects the calibration. A study by McKee-Cox (1974) showed that light does leak out the sides of finite cubic clouds. Figure 4 shows a graph from their report showing the comparison of the infinite horizontal extent cloud and the finite cubic cloud using a Monte Carlo multiple scattering technique. When the doubling method multiple scattering intensities used in this study are converted into the directional reflectance to conform to the convention of McKee and Cox, the doubling results agree closely with the infinite case of the Monte Carlo results. A study by Mosher (1975) on the determination of infrared emissivity of clouds using the visible brightness indicated that the calibration factor α determined by bright clouds might be too high because of the problem of light escaping from the sides of the clouds. In the brightness normalization program, the calibration factor α can be lowered by the user. This has the effect of lowering the intensity vs. optical thickness curves toward what might be expected of finite clouds.

ACKNOWLEDGEMENT

This work was supported by NOAA Grant 04-3-158-61.

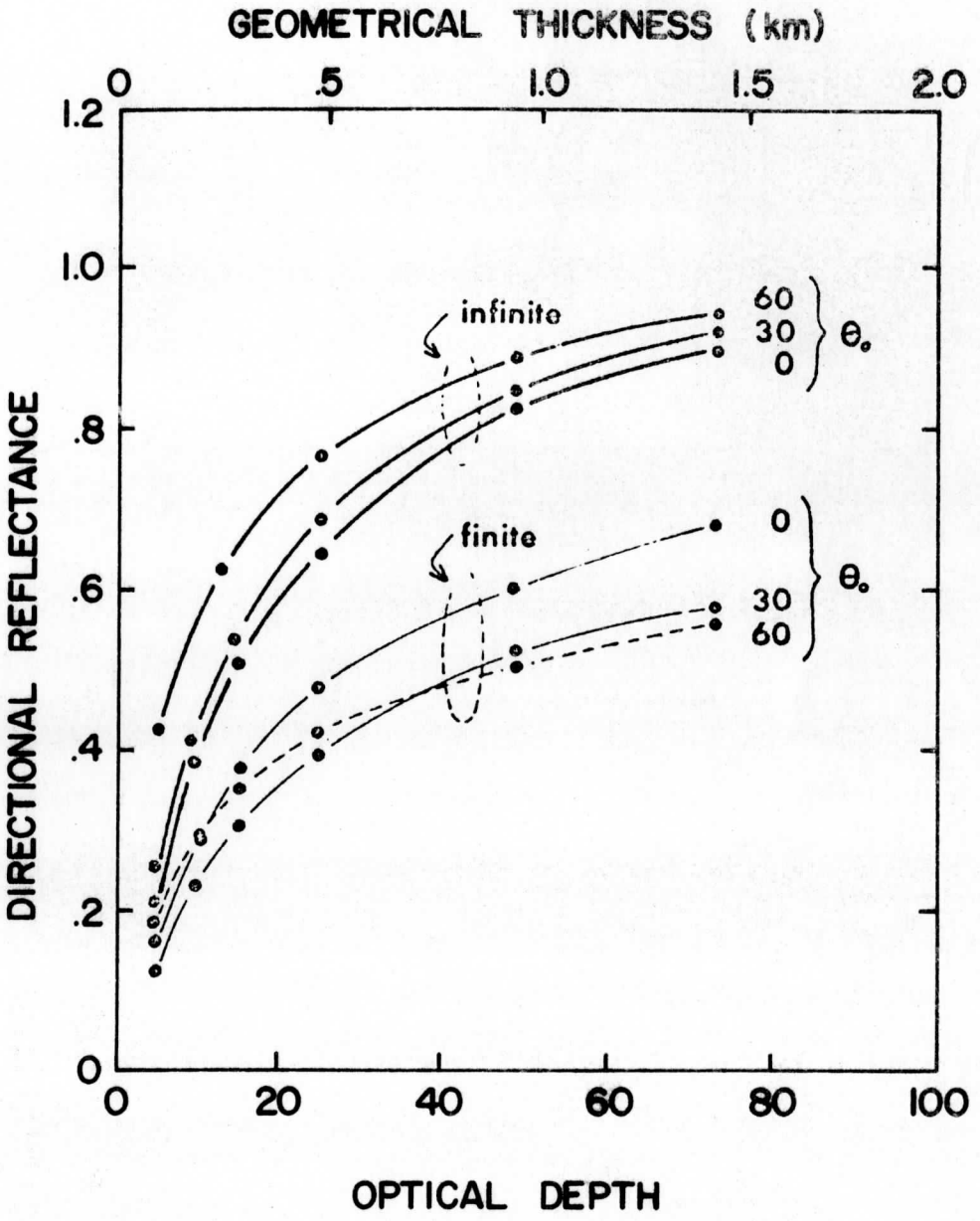

Figure 4 DIRECTIONAL REFLECTANCE OF INFINITE CLOUDS AND FINITE CUBIC CLOUDS (FROM McKEE AND COX, 1974).

REFERENCES

Bartman, Fred L., 1967: "The Reflectance and Scattering of Solar Radiation by the Earth," NASA Report NAS-54(03).

Brennan, B. and W. R. Bandeen, 1970: "Anisotropic Reflectance Characteristics of Natural Earth Surfaces," Appl. Optics, 9, 405-412.

Diem, M.: "Messungen der Grösse von Wolkenelementen II." Meteor. Rund., 1, 266-273.

Griffith, Cecelia G. and William Lee Woodley, 1973: "On the Variation with Height of the Top Brightness of Precipitating Convective Clouds," J. Appl. Meteor., 12, 1086-1089.

Hansen, J. E., 1971a: "Multiple Scattering of Polarized Light in Planetary Atmospheres, Part I, The Doubling Method," J. Atmos. Sci., 28, 120-125.

_____, 1971b: "Multiple Scattering of Polarized Light in Planetary Atmospheres, Part II, Sunlight Reflected by Terrestrial Water Clouds," J. Atmos. Sci., 28, 1400-1426.

Hanson, K. J. and V. E. Suomi, 1968: "The Inspace, Absolute Calibration of ATS-I Cloud Camera," Studies in Atmospheric Energetics Based on Aerospace Probing, Annual Report-1967 on ESSA contract WBG-27, Department of Meteorology, University of Wisconsin.

Irvine, William M. and James B. Pollack, 1968: "Infrared Optical Properties of Water and Ice Spheres," Icarus, 8, 324-360.

Martin, David W. and Verner E. Suomi, 1972: "A Satellite Study of Cloud Clusters Over the Tropical North Atlantic Ocean," Bull. Amer. Meteor. Soc., 53, 135-156.

McKee, Thomas, B. and Stephen K. Cox, 1974: "Scattering of Visible Radiation by Finite Clouds," J. Atmos. Sci., 31, 1885-1892.

Meteorology of the Near Future Prospects of Image Pattern Recognition, Report of the Workshop held at NASA, Goddard Space Flight Center 11 November 1974.

Mosher, F. R., 1975: SMS Cloud Heights in Man-Computer Interactive Data Access System (McIDAS), Final Report Contract NAS5-23296.

Payne, Richard E., 1972: "Albedo of the Sea Surface," J. Atmos. Sci., 29, 959-970.

Ruff, I., R. Koffler, S. Fritz, J. S. Winston, and P. K. Rao, 1963: "Angular Distribution of Solar Radiation Reflected from Clouds as Determined from TIROS IV Radiometer Measurements," J. Atmos. Sci., 25, 323-332.

Sikula, Gerald J. and Thomas H. Vonder Haar, 1972: "Very Short Range Local Area Weather Forecasting Using Measurements from Geosynchronous Meteorological Satellites," Colorado State University Atmospheric Science Paper No. 185, Air Force Contract No. F19628-71-C-0073.